AD NUMBER

AD876989

NEW LIMITATION CHANGE

TO

Approved for public release, distribution unlimited

FROM

Distribution authorized to U.S. Gov't. agencies and their contractors; Critical Technology; OCT 1970. Other requests shall be referred to Naval Ship Research and Development Center, Attn: Code 700, Washington DC 20350.

AUTHORITY

DWTNSRDC ltr, 23 Mar 1984
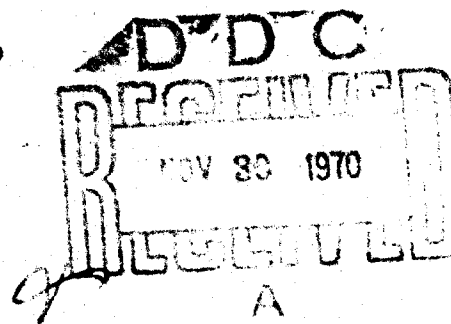
AD 876989

NAVAL SHIP RESEARCH AND DEVELOPMENT CENTER

Washington, D.C. 20034

THE EFFECT OF RESIDUAL STRESSES ON THE BUCKLING

STRENGTH OF FABRICATED HY-80 STEEL

HEMISPHERICAL SHELLS

by

M.G. Costello

D D C

NOV 30 1970

A

STRUCTURAL MECHANICS LABORATORY

RESEARCH AND DEVELOPMENT REPORT

October 1970

Report 3407

THIS REPORT HAS BEEN DELIM.TED

AND CLEARED FOR PUBLIC RELEASE

UNDER DOD DIRECTIVE 5200.20 AND

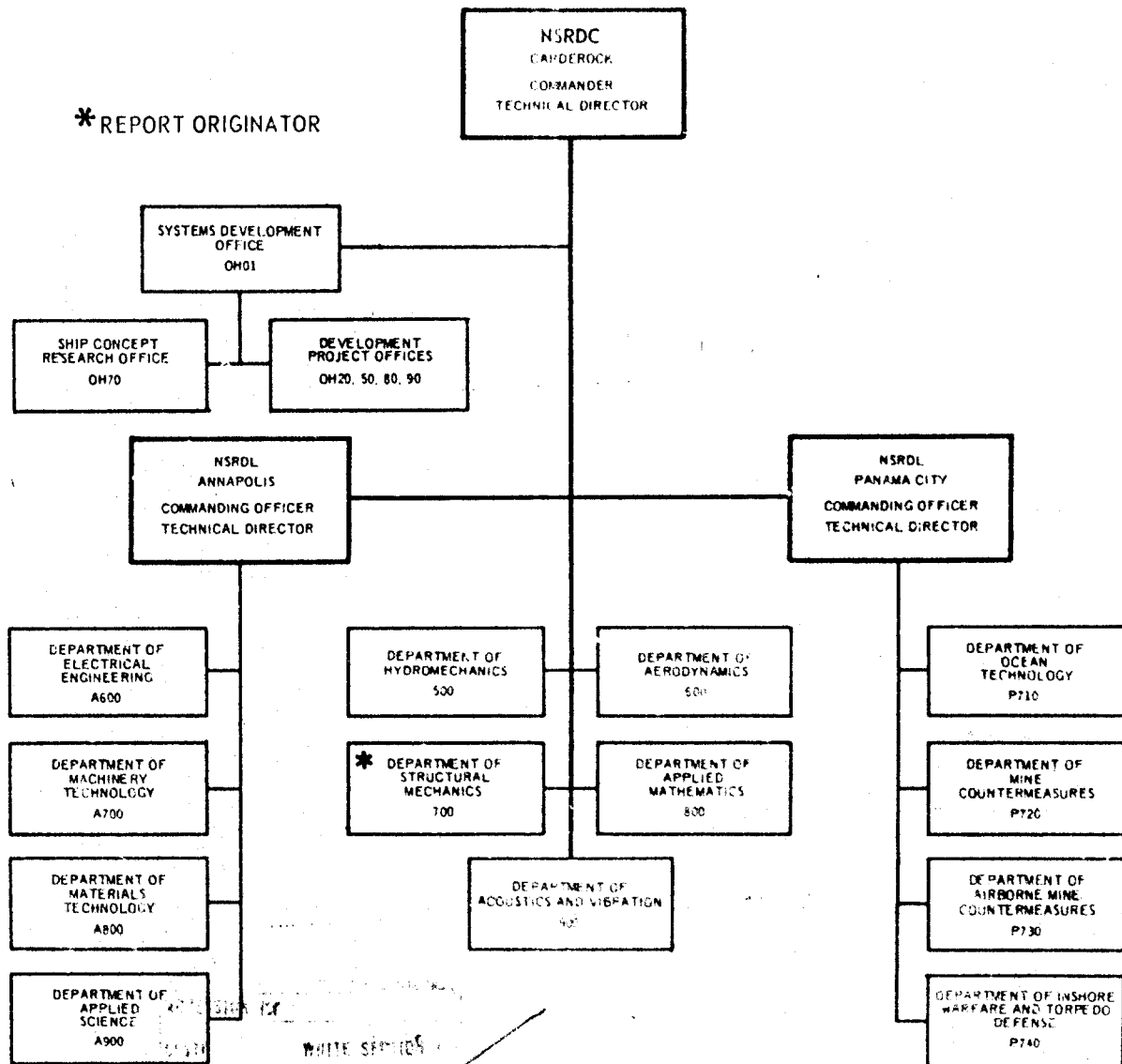NO RESTRICTIONS ARE IMPOSED UPON

ITS USE AND DISCLOSURE.

DISTRIBUTION STATEMENT A

APPROVED FOR PUBLIC RELEASE;

DISTRIBUTION UNLIMITED.

MAJOR NSRDC ORGANIZATIONAL COMPONENTS

NSRDC
CARDEROCK
COMMANDER
TECHNICAL DIRECTOR

✱ REPORT ORIGINATOR

SYSTEMS DEVELOPMENT OFFICE
OH01

SHIP CONCEPT RESEARCH OFFICE
OH70

DEVELOPMENT PROJECT OFFICES
OH20, 50, 80, 90

NSRDL ANNAPOLIS
COMMANDING OFFICER
TECHNICAL DIRECTOR

NSRDL PANAMA CITY
COMMANDING OFFICER
TECHNICAL DIRECTOR

DEPARTMENT OF ELECTRICAL ENGINEERING
A600

DEPARTMENT OF HYDROMECHANICS
500

DEPARTMENT OF AERODYNAMICS
600

DEPARTMENT OF OCEAN TECHNOLOGY
P710

DEPARTMENT OF MACHINERY TECHNOLOGY
A700

✱ DEPARTMENT OF STRUCTURAL MECHANICS
700

DEPARTMENT OF APPLIED MATHEMATICS
800

DEPARTMENT OF MINE COUNTERMEASURES
P720

DEPARTMENT OF MATERIALS TECHNOLOGY
A800

DEPARTMENT OF ACOUSTICS AND VIBRATION
900

DEPARTMENT OF AIRBORNE MINE COUNTERMEASURES
P730

DEPARTMENT OF APPLIED SCIENCE
A900

DEPARTMENT OF INSHORE WARFARE AND TORPEDO DEFENSE
P740

DEPARTMENT OF THE NAVY

NAVAL SHIP RESEARCH AND DEVELOPMENT CENTER

WASHINGTON, D.C. 20034

THE EFFECT OF RESIDUAL STRESSES ON THE BUCKLING

STRENGTH OF FABRICATED HY-80 STEEL

HEMISPHERICAL SHELLS

by

M.G. Costello

October 1970   Report 3407

TABLE OF CONTENTS

LIST OF FIGURES

LIST OF TABLES

ABSTRACT

Hydrostatic tests were conducted on nine fabricated
HY-80 steel hemispheres to observe the effects of residual
stresses from cold forming and welding on elastic response
and collapse strength. Nondimensionalized collapse data
indicated that residual stresses due to welding play a sig-
nificant part in the collapse strength of fabricated HY-80
steel hemispheres.

ADMINISTRATIVE INFORMATION

INTRODUCTION

For several years the Naval Ship Research and Development Center
(NSRDC) has been studying realistically fabricated hemispherical shells in
order to determine the individual contributions of such factors as local
flat spots and thin spots, mismatch at joints, residual stresses, and
boundary conditions to the observed reduction in strength of these shells
as compared with perfect hemispheres. Tests have been conducted on both
30- and 66-in. diameter HY-80 hemispheres fabricated by welding together
six doubly curved "orange peel" shell segments plus a shallow polar cap.
Some of these hemispheres were hydrostatically tested in the as-fabricated
condition while others were stress relieved prior to hydrostatic testing.
Comparison of test results[1,2] indicated an appreciable difference in col-
lapse strengths attributable to the weakening effects of residual stresses,
first from cold forming the individual segments and second from welding the
segments together. Since forming stresses can be eliminated on prototype
hulls by stress relieving the segments or by using hot forming practices,
the project herein reported was initiated to determine the effect of weld-
ing residual stresses alone.

Seven 66-in. diameter and two 30-in. diameter hemispheres were
fabricated and tested. Of the 66-in. diameter hemispheres, three, AF-1,

---

[1]References are listed on page 51.

1

AF-2, and AF-3, were tested in the as-fabricated (cold formed) condition while the segments for the other four, SRS-1, SRS-2, SRS-3, and SRS-4, as well as the two 30-in. diameter hemispheres SRS-2A and SRS-3A, were stress relieved after light tack welding and before final welding. The as-fabricated models were made to supplement previous test data.

DESCRIPTION OF MODELS

Seven 66-in. diameter HY-80 steel hemispheres were made by the Lukens Steel Company using procedures used for full-scale submarine bulkheads. Except where noted, the methods were the same as used for the 66-in. diameter hemispherical models reported in References 1 and 2. Each of the present models consisted of six 60-deg "orange peel" segments and one shallow spherical cap, all formed from pieces of the same flat plate. An assembled hemisphere is shown in Figure 1. Models AF-1, AF-2, and AF-3 were made by cold forming the individual segments and welding them together. Models SRS-1, SRS-2, SRS-3, and SRS-4 were made by hot forming the individual segments, lightly tack welding them in place, stress relieving for an hour at 1025 deg, and finally welding the segments.

Models SRS-2A and SRS-3A, 30-in. diameter HY-80 hemispheres, were made at NSRDC. The segment configuration was the same as for the 66-in. diameter hemispheres. The individual segments were cold formed, lightly tacked to their mold and stress relieved at 1025 deg for an hour. The stress relieved segments were then welded together.

In the case of the two 30-in. models, SRS-2A and SRS-3A, two extra "orange peel" segments were cut from the same plates and cold formed. Compression specimens were cut from one segment. The other segment was stress relieved with its model after which compression specimens were taken. The yield strength distribution for these extra segments is shown in Figure 2. Typical stress-strain curves for model SRS-2A from the original flat plate and the two extra formed segments are shown in Figure 3.

For all calculations Young's modulus and Poisson's ratio were assumed to be 30×10^6 psi and 0.3, respectively. For all models the yield strength σ_y of the original plate was used in calculations for the collapse pressure. It is realized that this will not be representative of the

2

material in place for the three AF models because of work hardening. Data on the variation in yield strength due to forming and stress relieving is presented in Table 1.

Prior to testing each hemispherical model was welded to a stiffened cylinder. The cylinders used on the 66-in. and 30-in. hemispheres were made from HY-80 and HY-150 steel respectively for two previous series of hemispheres. Although the cylinders did not provide membrane boundaries at the hemisphere-cylinder juncture, it was felt that the stiffnesses would be sufficiently close to preclude any detrimental effects. Model and cylinder assemblies are shown in Figure 1 together with nominal dimensions.

PROCEDURE

DETERMINATION OF INITIAL IMPERFECTIONS

The analysis for imperfect spherical shells[3] requires the determination of local imperfections over the entire shell surface. This was accomplished by measuring deviations from an assumed radius using an assumed center as reference. This data was fed into a computer program, YL01, which calculated a new center and new average radius and modified the deviations accordingly. These deviations were plotted in the form of contour maps as shown in Figure 4. Minus signs indicate inward deviations. The view is of the inside of the model rolled out into a flat surface whose radial scale remains constant. The scale factor is found by dividing one half of the circumference of the hemisphere by the diameter of the plotted circle. The scale in all other directions is a function of orientation and distance from the center of the plot. To overcome the mapping problem clear plastic overlays such as shown in Figure 5 were used. Any diagonal across an oval represents the same arc length on the hemisphere.

In addition to sphericity readings 151 thickness readings were made on each shell. They are presented in Table 2.

The contour map, overlay, and thickness table were used to examine flat spot areas. The method is described in detail in References 1 and 3. Each flat spot was characterized by its ratio of local to nominal radius R_1/R and its local thickness h_a.

3

In addition to flat spots, mismatches at welded joints in terms of deviations from sphericity are given in Figure 4.

Recently the examination of flat spots has been automated. A computer program, OSR1, written by R.D. Rockwell of NSRDC incorporates YL01 but requires the additional input of thickness measurements. Output includes the contour map which was heretofore plotted by hand and a table of local radii.

TEST PROCEDURE

Each hemisphere was instrumented with between 50 and 150 foil-resistance strain gages. Areas for gaging were chosen on the basis of flat spot calculations and mismatch readings. Additional gages were placed at the edges of segments for the SRS models to detect the effect of welding residual stresses. Strain gage locations are shown in Figure 6.

The 66-in. and 30-in. models were statically tested in oil in the NSRDC 6-foot head testing tank and 4-foot testing tank, respectively. The test setup is shown in Figure 7. In most cases each test consisted of three pressure runs--the first and second to approximately 70 and 90 percent, respectively, of the collapse pressure and the third to collapse. The final increment prior to collapse was less than 2 percent of the collapse pressure.

RESULTS AND DISCUSSION

Experimental collapse pressures for each model are shown in Table 3. Figure 6 shows strain sensitivities defined by the slope of the initial linear portion of the applied pressure versus measured strain curve and given in μin./in./psi.

Typical pressure-strain plots are presented in Figure 8. Pressure-strain data for Model SRS-1 is not available for presentation. For such an unstable model it is unlikely that strain gages at local flat spots experienced appreciable nonlinearity prior to collapse. Model SRS-2 is also not included. For this model all gages were linear up to collapse. Figure 9 shows the models after collapse.

4

Nondimensional plots of experimental results for the nine models are presented in Figure 10; the abscissa is the ratio of elastic buckling pressure P_3' to the yield pressure P_y', and the ordinate is the ratio of the experimental collapse pressure P_c to P_y'. It should be noted that local geometry in the area of failure was used to calculate P_3' and P_y', which are defined by the expressions

$$P_3' = 0.84E \left(\frac{h_a}{R_{10}}\right)^2 \text{ for } \nu = 0.3 \tag{1}$$

$$P_y' = \frac{2 \sigma_y h_a R_{1m}}{(R_{10})^2} \tag{2}$$

where h_a is the average thickness at the flat spot,

R_{10} is the local outside radius,

R_{1m} is the local midsurface radius,

E is Young's modulus, and

σ_y is the yield strength.

Results of References 1 and 2 have been included for comparison. The difference between the yield line and the lower bound for the stress relieved models of References 1 and 2 was attributed to secondary moments. The difference between the lower bounds for the previous stress relieved models and the present models composed of stress relieved segments (SRS) is attributed to residual welding stresses. The difference between the lower bounds for the SRS models and the models tested in the as-fabricated (AF) state is attributed to residual forming stresses. The present results for the three as-fabricated models are consistent with previous results. The data point for AF-2 lies on the previously determined lower bound curve for as-fabricated hemispheres. AF-2 failed near a meridional weld. The data points for AF-1 and AF-3 however are considerably above the lower bound line. These two models failed in the middle of "orange peel" segments. A certain amount of scatter is evident in the data points for the six models composed of stress relieved segments. SRS-3A for example proved stronger than a comparable hemisphere without residual welding

5

stresses. The lower bound curve for these six models is somewhat lower than one might expect. It appears that removing the residual forming stresses does not do as much to increase the buckling pressure as does removing the residual welding stresses. The failure areas for all but SRS-4 of these six models were near welded joints.

Local fabrication mismatch between adjoining segments of the 66-in. diameter hemispheres was 0.1 inch or less. Mismatch for the 30-in. diameter hemispheres was 0.04 inch or less. This amounted in some cases to as much as 26 percent of the shell thickness. Although this sounds excessive it should be mentioned that the severity of the mismatch was always limited to a fraction of the length of the connection. None of the most severe mismatches as shown in Figure 4 are within the failure areas. The effect of mismatch alone on the collapse strength of hemispherical shells has been investigated and the results presented in Reference 4.

As is readily apparent from Table 4 only three of the nine models of this series collapsed at area I, the geometrically "critical" area based on minimum h_a/R_1. This is attributed to such factors as variations in residual stress, yield strength, the shape of the stress-strain curve and the shape of the flat spots which are neglected in the present analysis. Prior to destructive testing one must assume that failure will occur at area I. The predicted collapse pressure, P_{pred}, is thus based on the local geometry of area I. Should failure occur at a less "critical" flat spot the analysis becomes more conservative. Table 4 shows values of P_{pred} for the present series of models and compares them with the experimental collapse pressures P_{exp}.

Although both areas I and VI were within the failure area of SRS-2, area VI was used for the collapse calculations for two reasons. First, area VI was the closest to the center of the failure area and second, no non-linearity of strains was recorded at area I just prior to failure. Because of its relatively low R_1/R ratio no strain gages were placed at area VI.

Measured maximum membrane stress sensitivities are compared with their theoretical or calculated counterparts at several flat spot areas for each model in Table 3. Equations defining the two stress sensitivities are also given in the table. With few exceptions agreement between the

6

two was within 10 percent with the calculated value usually greater than the measured value. Looking at the exceptions in Table 3 in all but one case, SRS-3 area V where all measured strain sensitivities were somewhat suspect, the calculated stress was higher than the measured value.

CONCLUSIONS

1. Residual welding stresses appear to play a significant role in the collapse strength of HY-80 steel hemispheres. Nondimensionalized collapse data for hemispheres whose formed segments had been stress relieved prior to being welded together fell closer to the lower bound results for hemispheres tested in the as-fabricated condition than to the lower bound for completely stress relieved hemispheres.

2. The agreement between calculated and measured membrane stress sensitivities at flat spot areas was fairly good. With few exceptions agreement was within 10 percent.

ACKNOWLEDGMENTS

7
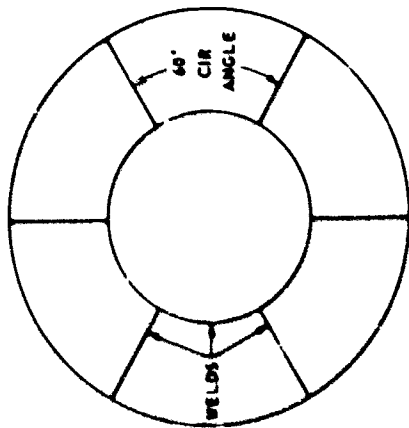
MODEL	a	b	c	d	e	f	g	hᵣ	i	j	m	n
AF-1	2 3/8	5/8	1/2		1/2	1 1/2	65	3/8	2 1/2	66		
AF-2	3	1	13/16		13/16	2	64 13/16	17/32	2 1/4	66		
AF-3	3	1	13/16		13/16	2	64 13/16	23/32	2 1/4	66		
SRS-1	2 3/8	5/8	1/2		1/2	1 1/2	65	1/4	2 1/2	66		
SRS-2	2 3/8	5/8	1/2		1/2	1 1/2	65	3/8	2 1/2	66		
SRS-3	3	1	13/16		13/16	2	64 13/16	17/32	2 1/4	66		
SRS-4	3 1/4	1 1/4	1 1/8		1 1/8	2 1/2	64 5/8	23/32	3 3/4	58 1/2		
SRS-2A	0.95	0.51	0.16	9.50	0.24	0.38	29.44	0.16	0.67	30.0	0.15	0.13
SRS-3A	1.20	0.65	0.30	0.82	0.42	0.55	29.44	1/4	1.00	30.0	0.25	0.20
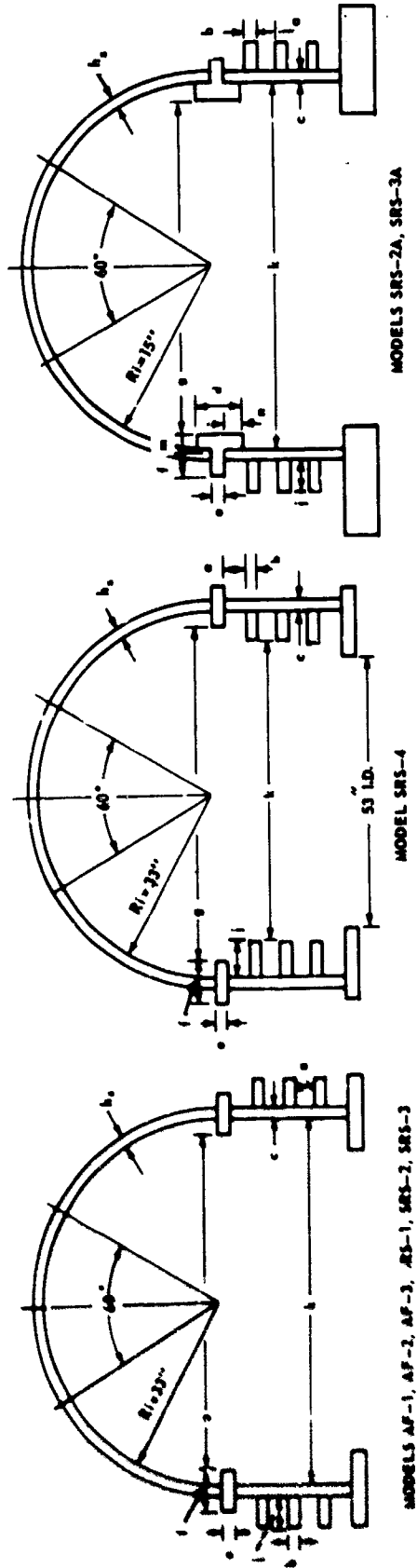
Figure 1 - Model and Cylinder Assembly

8
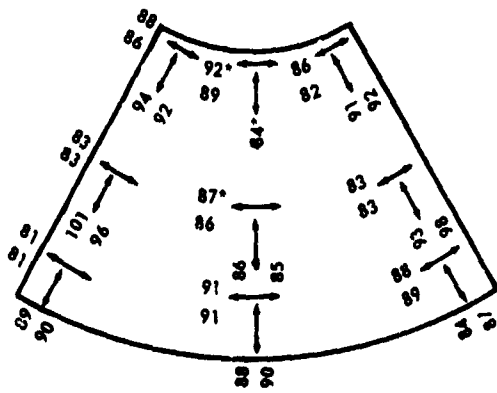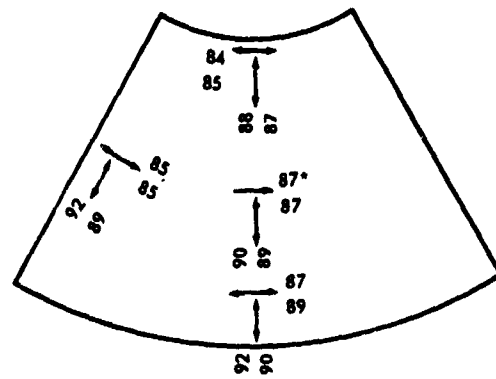
AS FABRICATED

STRESS RELIEVED

SRS-2A
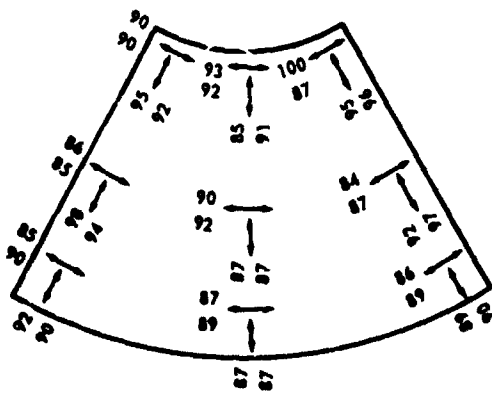
AS FABRICATED
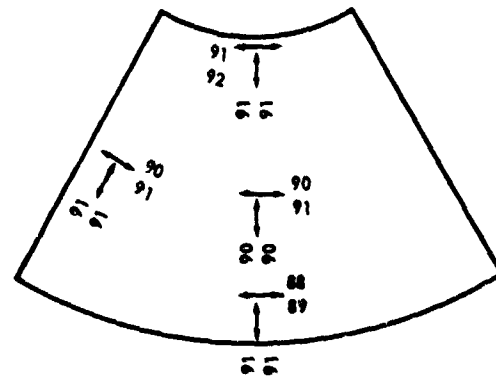
STRESS RELIEVED

SRS-3A

0.2 PERCENT YIELD STRENGTHS ARE IN KSI.
* PLOTTED IN FIGURE 3

Figure 2 - Yield Strength Distribution in As-Fabricated and
Stress Relieved Formed Segments for Models SRS-2A and SRS-3A

9
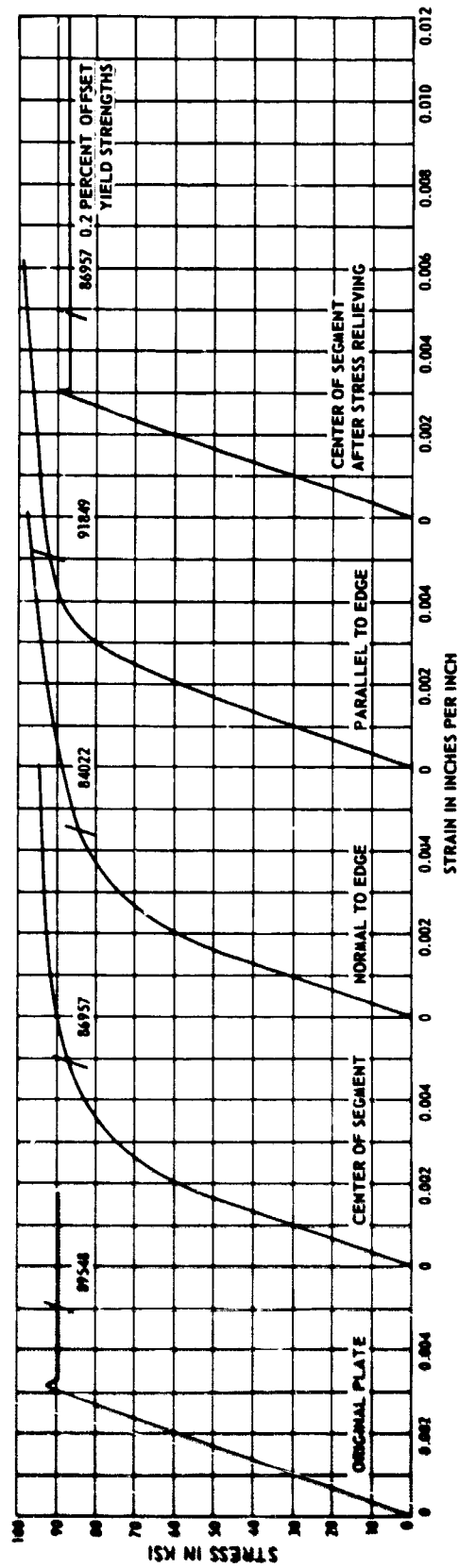
Figure 3 - Typical Stress-Strain Curves from Original Plate, Segment after
Forming, and Segment after Forming and Stress Relieving of Model SRS-2A

Figure 4 - Deviations from Sphericity

Figure 4a - Model AF-1
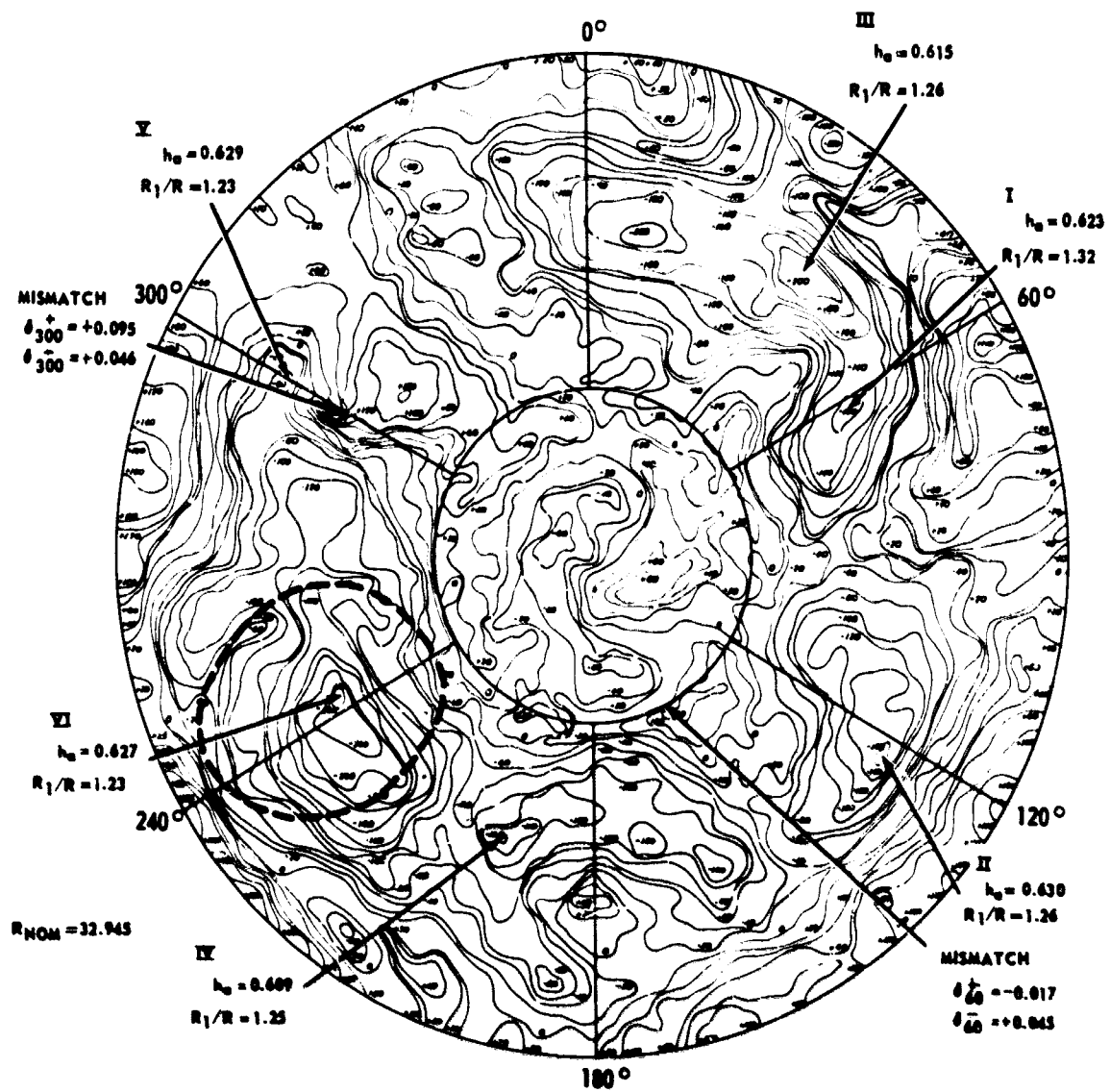
Figure 4b - Model AF-2

12
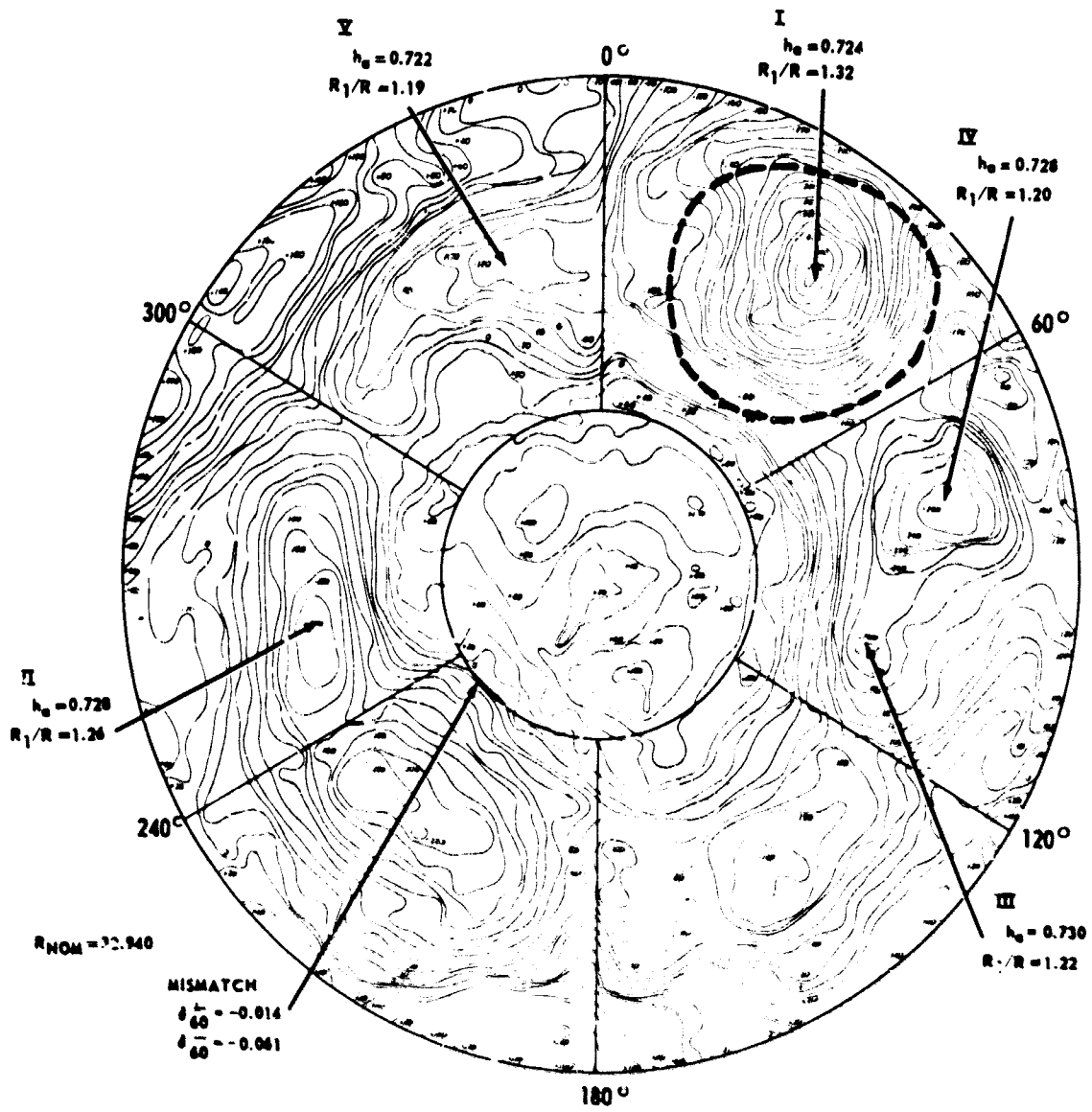
Figure 4c - Model AF-3

15
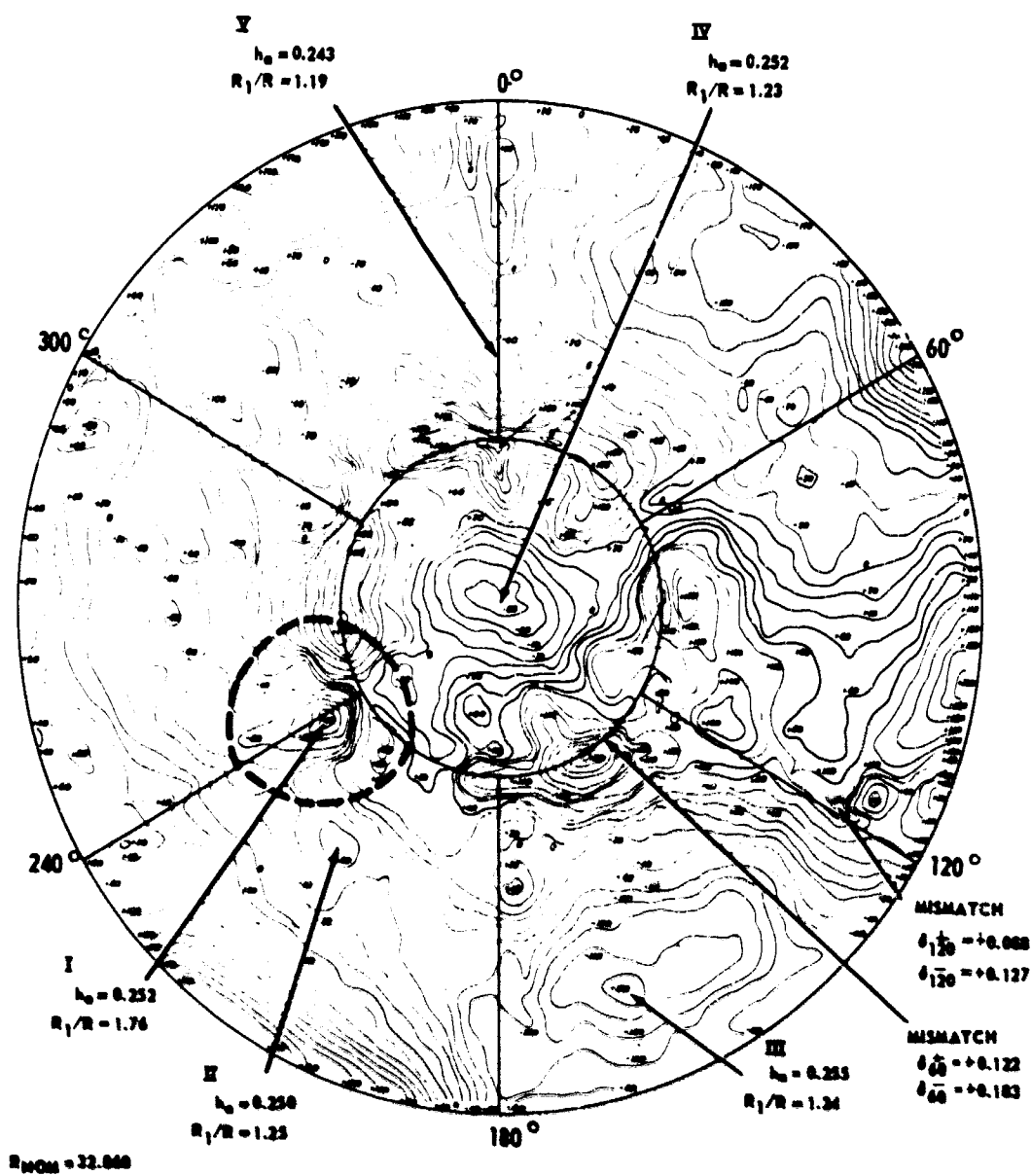
Figure 4d - Model SRS-1

14
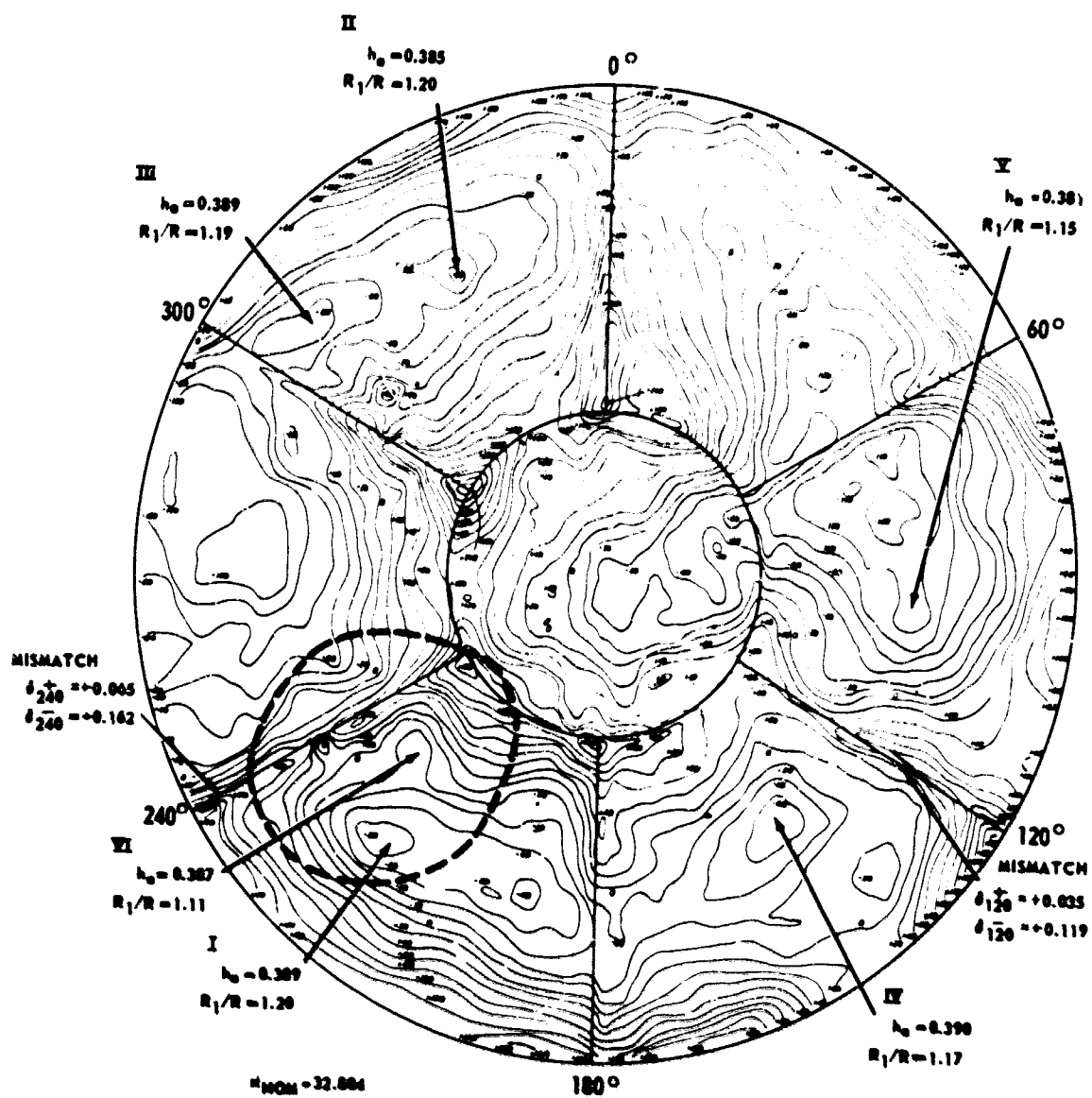
Figure 4e - Model SRS-2
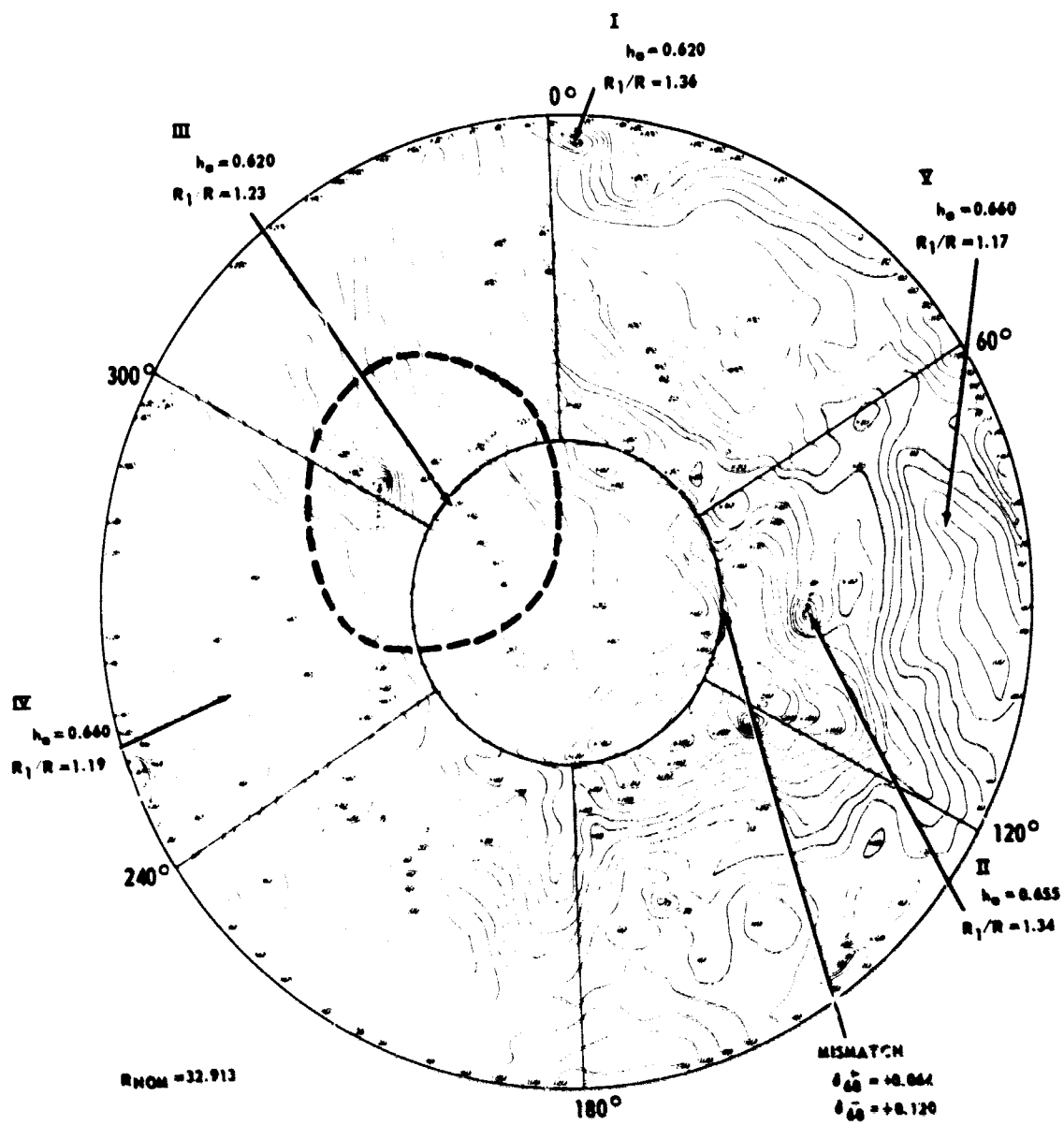
Figure 4f - Model SRS-3

16
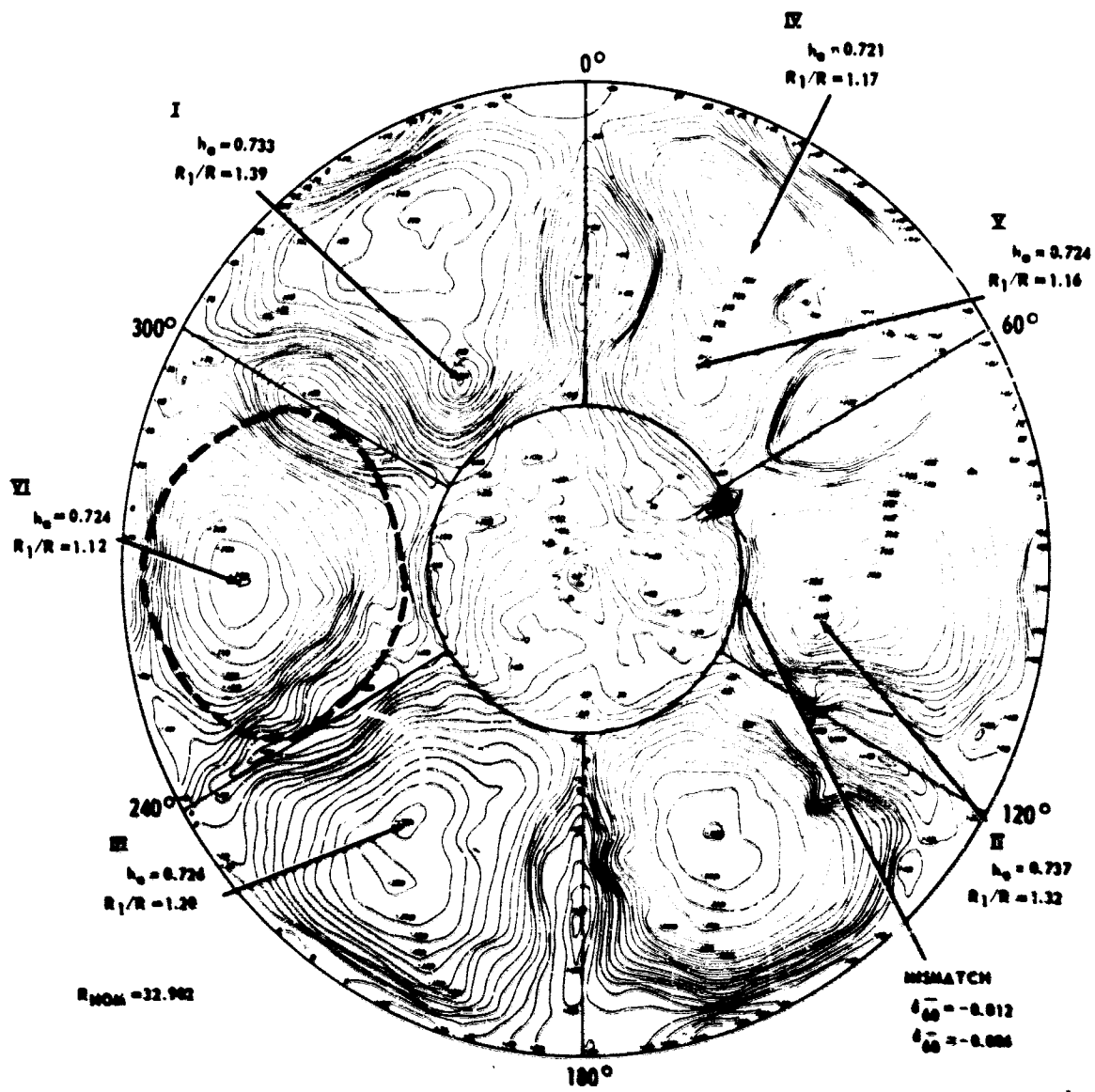
Figure 4g - SRS-4

Figure 4h - Model SRS-2A

16

II
$h_\alpha = 0.247$
$R_1/R = 1.13$

0°

MISMATCH
$\delta_{60}^+ = -0.004$
$\delta_{60}^- = +0.027$

MISMATCH
$\delta_{300}^+ = -0.018$
$\delta_{300}^- = +0.013$

300°

60°

V
$h_\alpha = 0.249$
$R_1/R = 1.10$

240°

IV
$h_\alpha = 0.247$
$R_1/R = 1.10$

120°

III
$h_\alpha = 0.248$
$R_1/R = 1.13$

I
$h_\alpha = 0.248$
$R_1/R = 1.17$

$R_{NOM} = 15.191$

180°
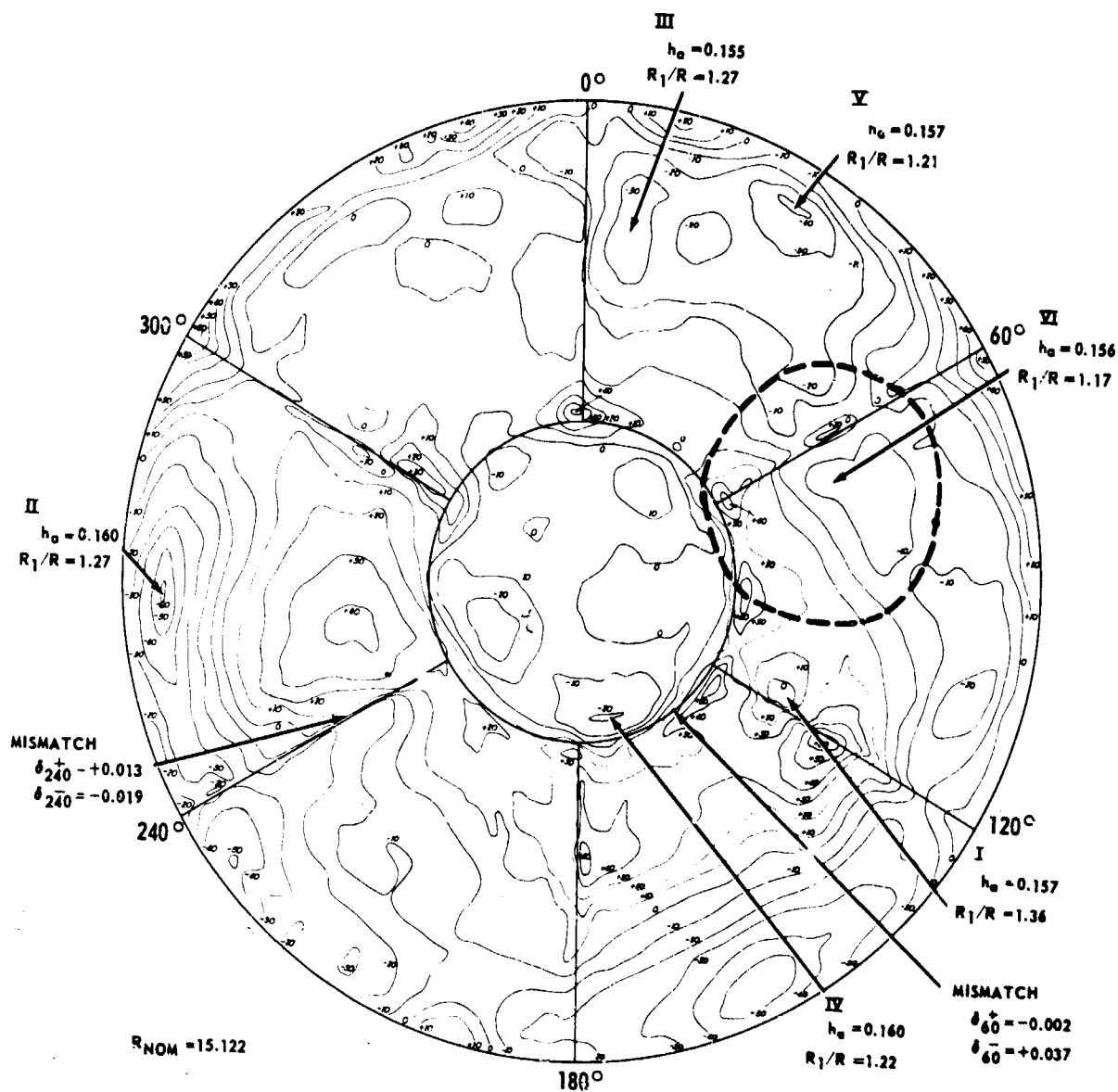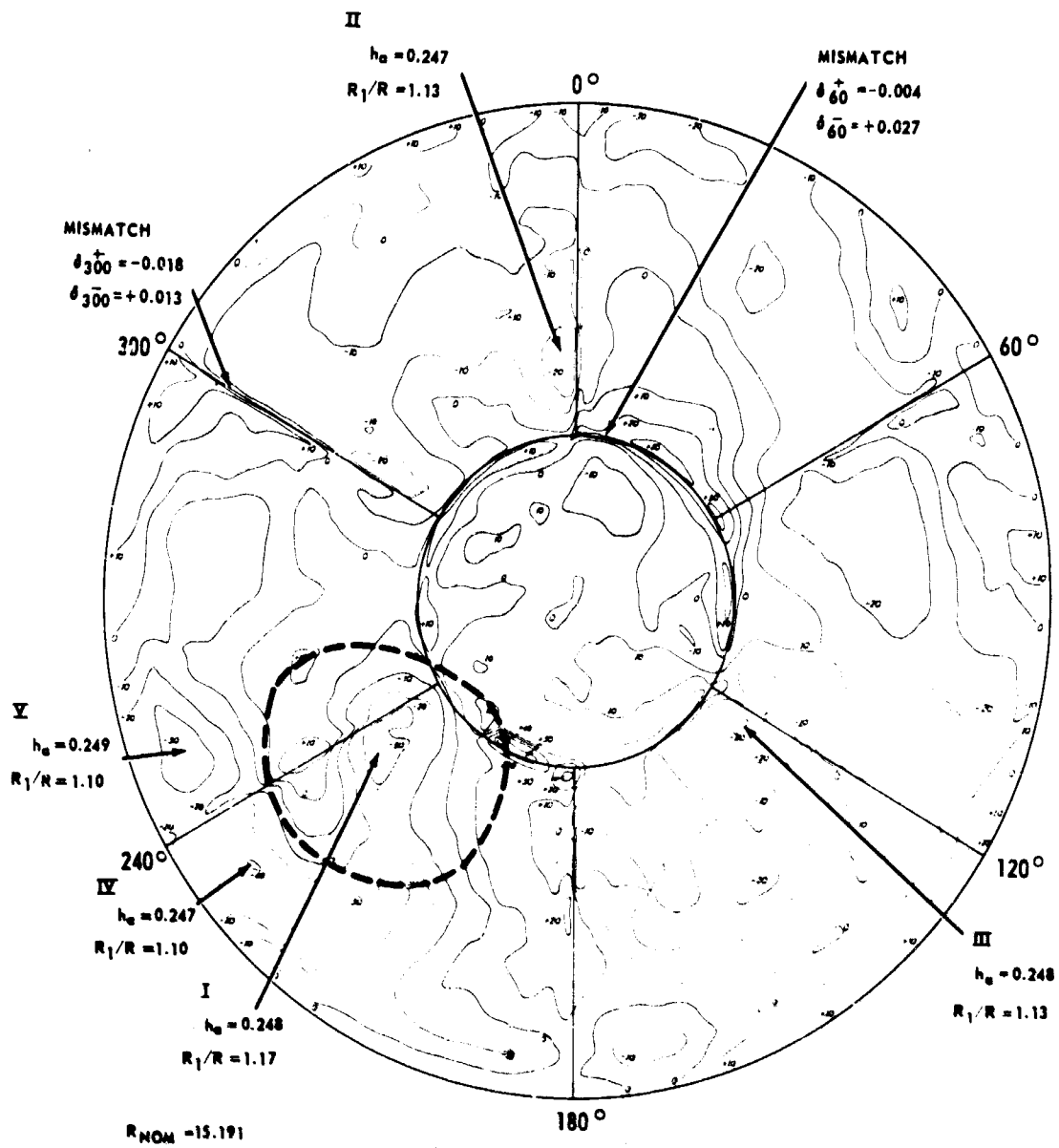
Figure 4i - Model SRS-3A

19
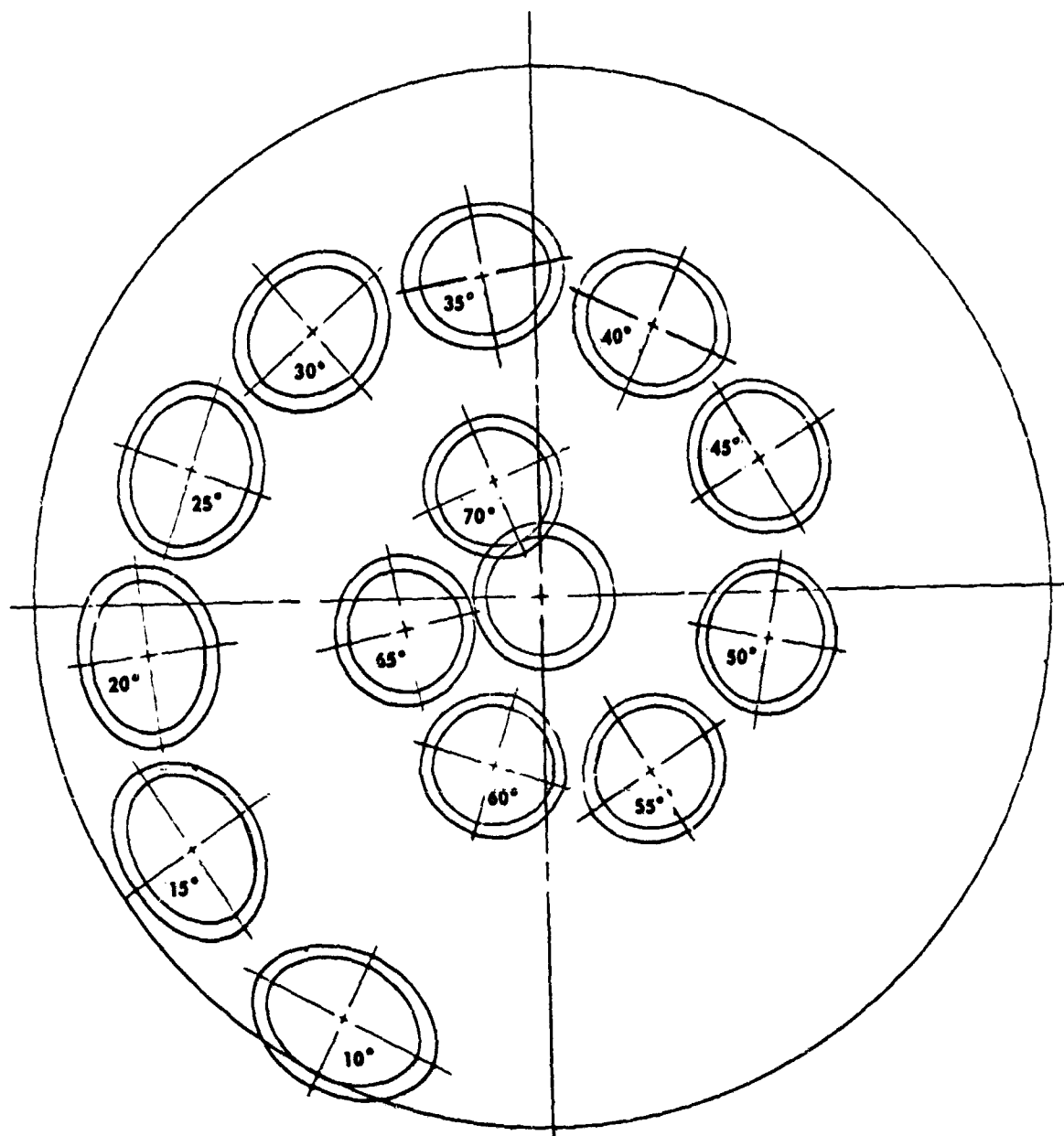
THE SURFACE ENCLOSED BY THE SOLID CIRCLE SHOWN REPRESENTS A
HEMISPHERE ROLLED OUT INTO A FLAT SURFACE WHOSE RADIAL SCALE
REMAINS CONSTANT.

Figure 5 - Arc Length Scales

Figure 6 - Strain Gage Locations and Strain Sensitivities

The layout shown represents a view looking into the open end of the model except where noted. Both inside and outside surfaces are instrumented for each position indicated. All inside gages have numbers begining with 200 and all outside with numbers begining with 100 (only the outside gages are indicated on these diagrams). All circumferential gage numbers end with an even number and all meridional gages with an odd number. All gages oriented 45 deg from these directions have numbers ending with the letter A. The strain sensitivity for each gage is given in parenthesis adjacent to the gage in μ in./in./psi. The figure on the left is the sensitivity for the outside and the right for the inside. * indicates gage for which pressure strain plots are shown on Figure 8. The area of failure is indicated by broken line.
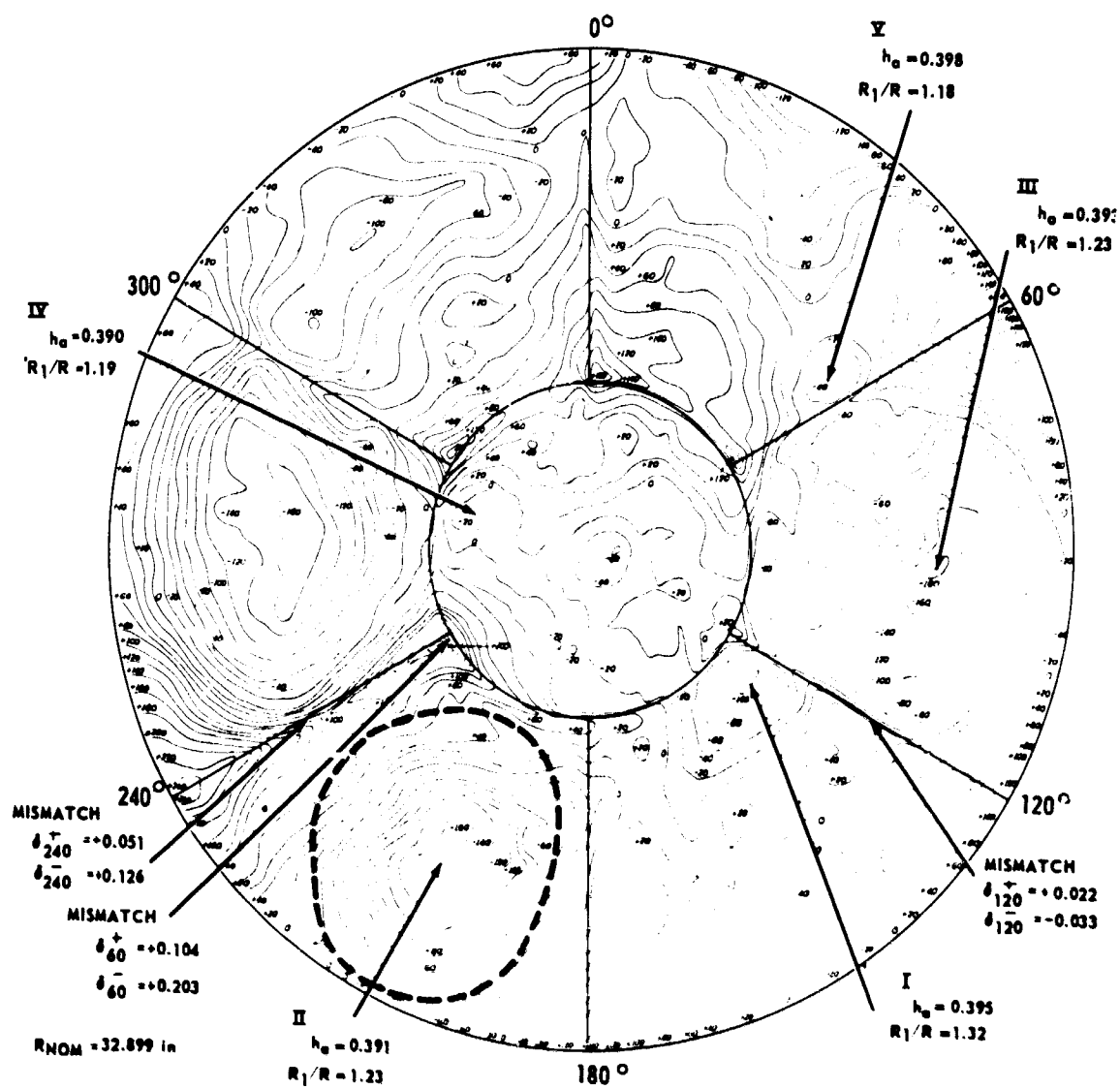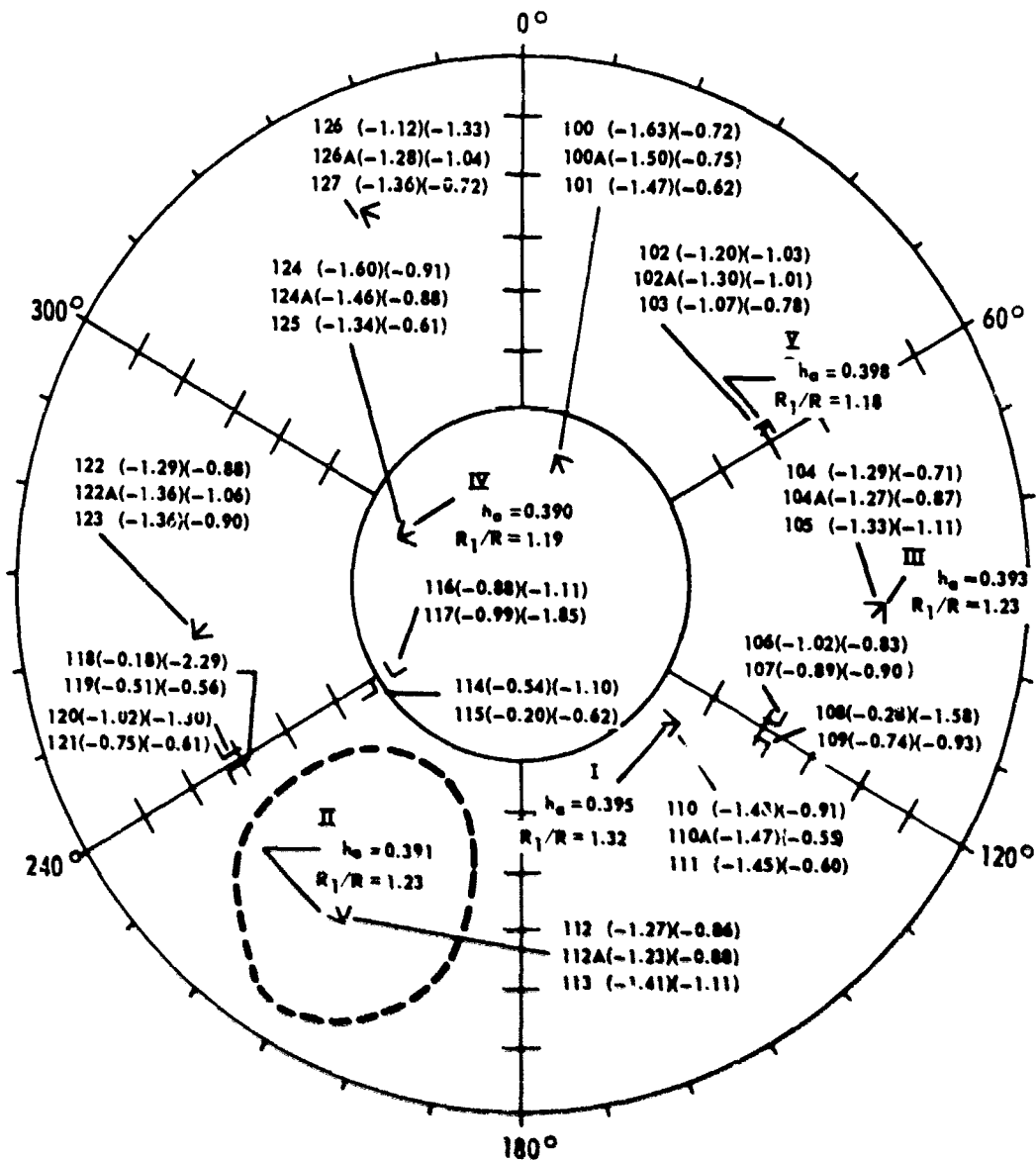

Figure 6a - Model AF-1
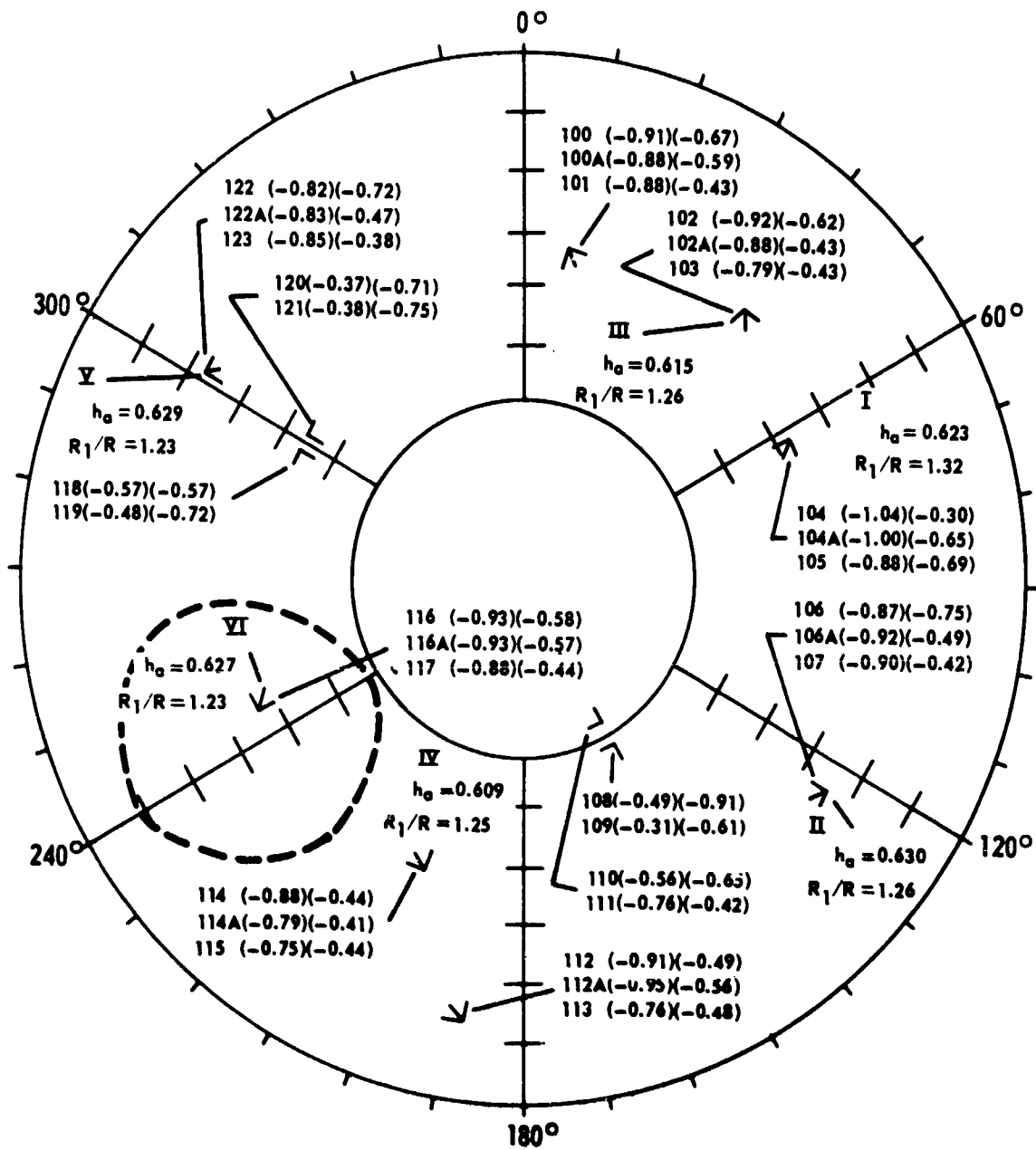
Figure 6b - Model AF-2

22
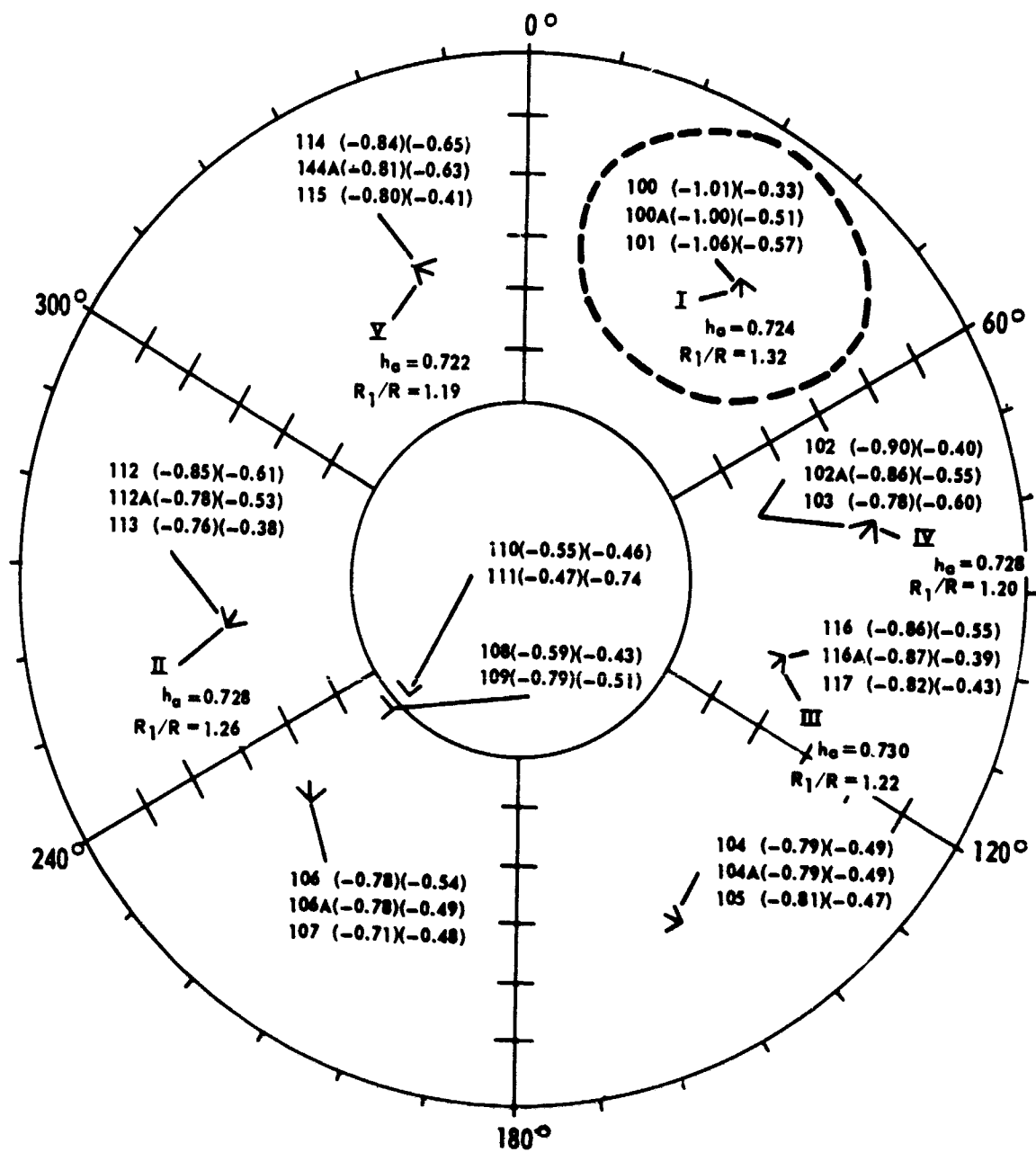
Figure 6c - Model AF-3

23
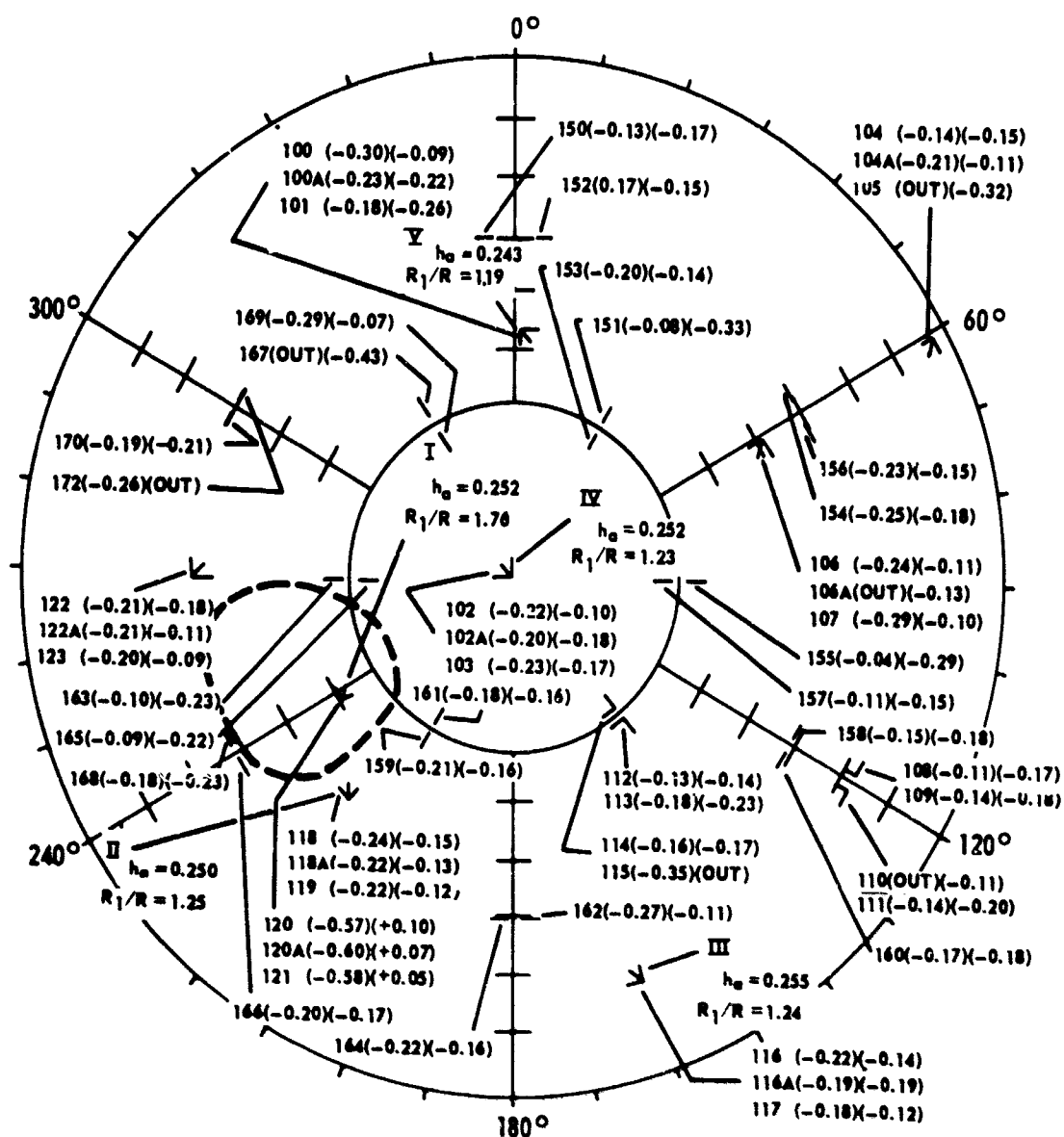
Figure 6d - Model SRS-1

24
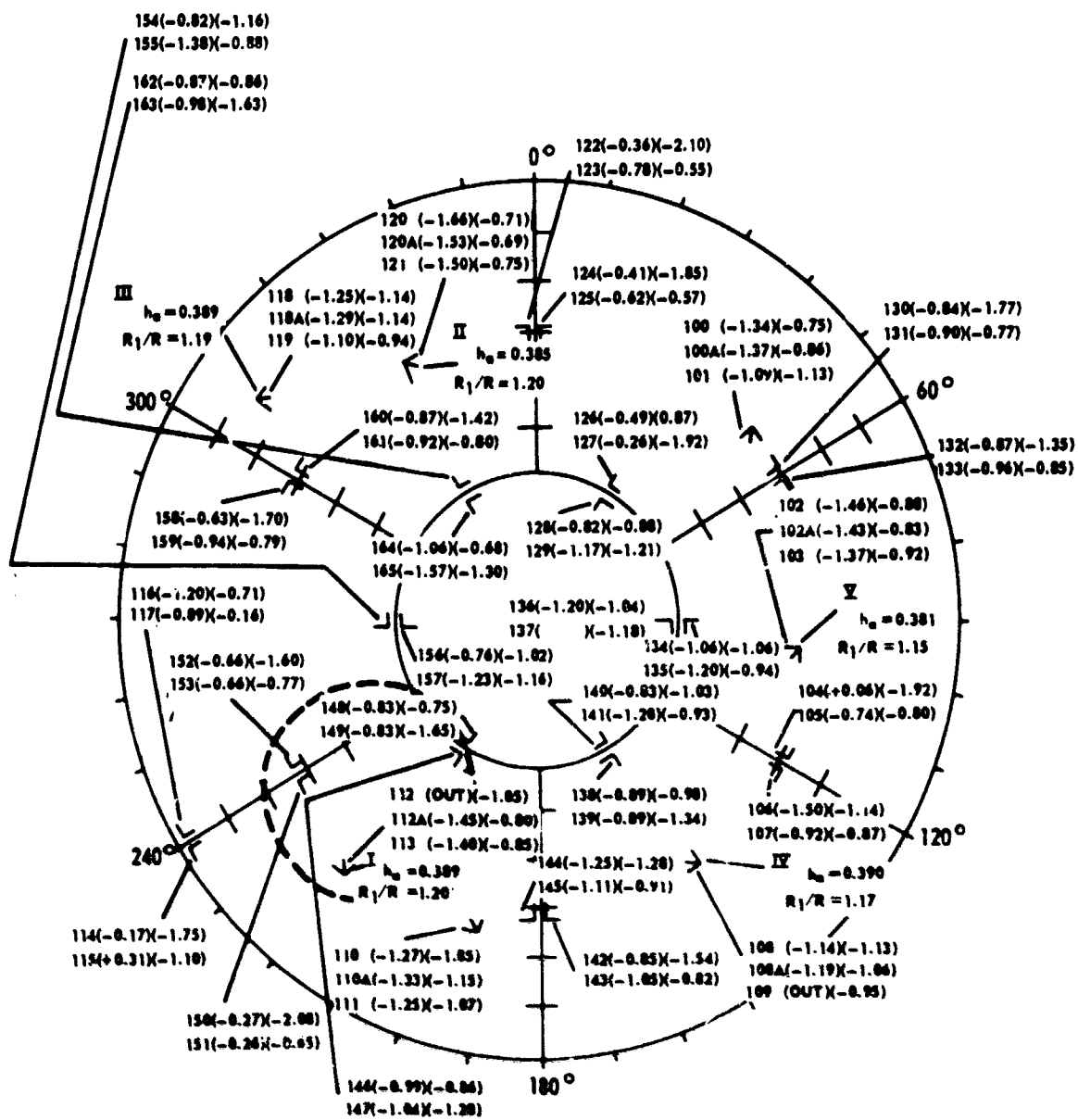
Figure 6e - Model SRS-2

25

Figure 6f - Model SRS-3
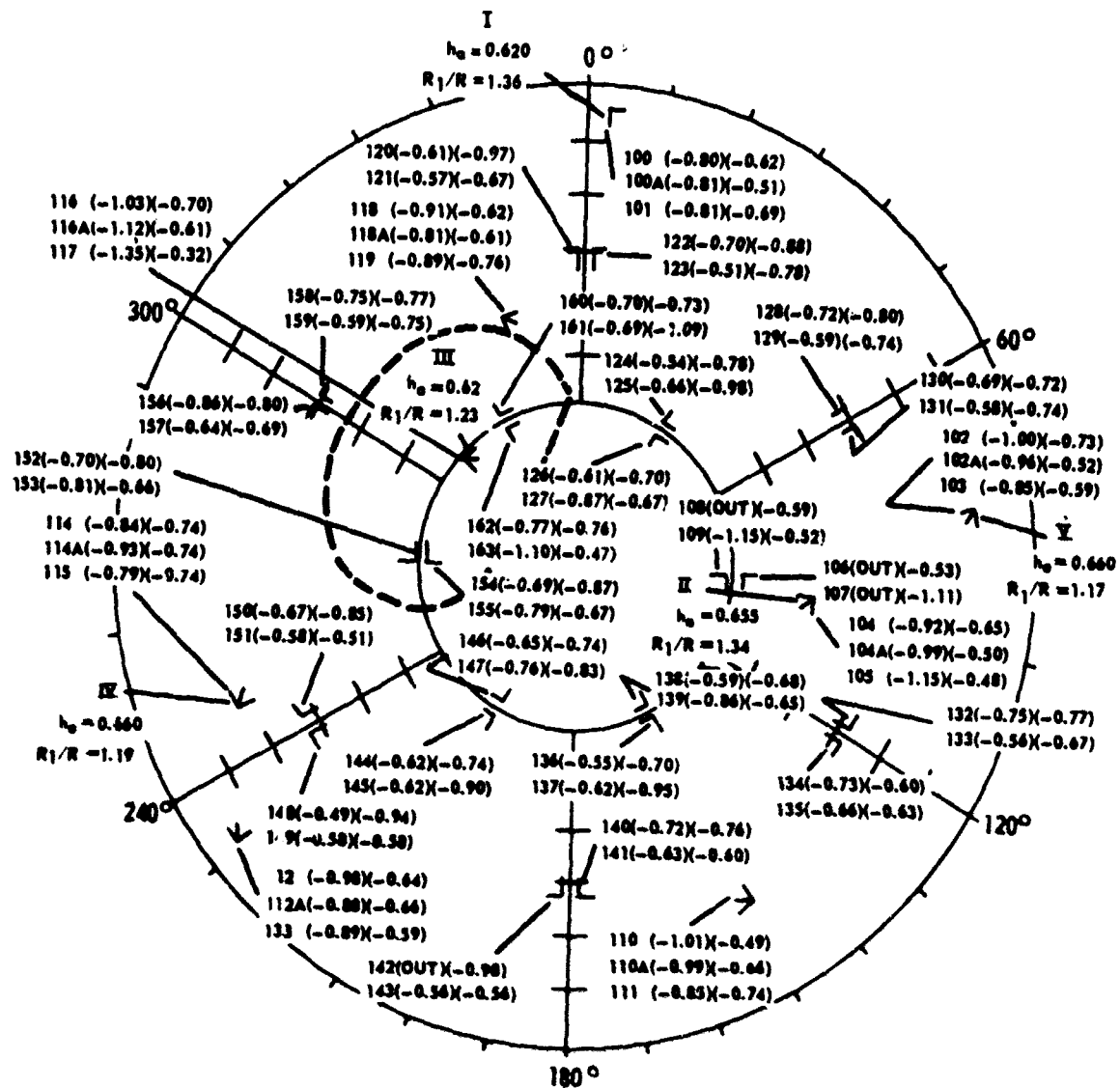
Notes:
1. View is looking down on the outside of the model.
2. Strain sensitivities for gages 100 through 134 are from the third pressure run only with recorded data modified to compensate for acostic gage behavior.

26
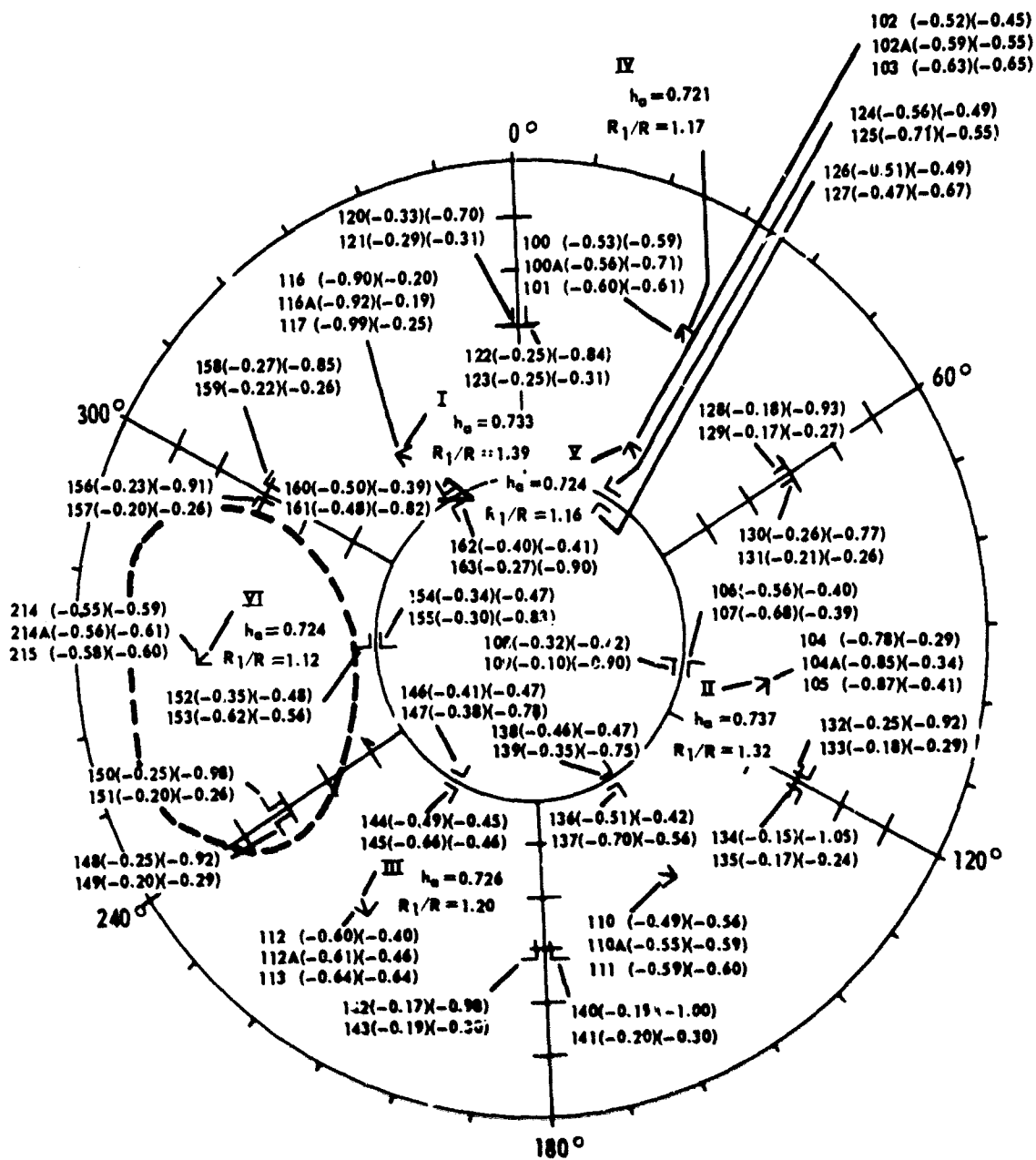
Figure 6g - Model SRS-4

27
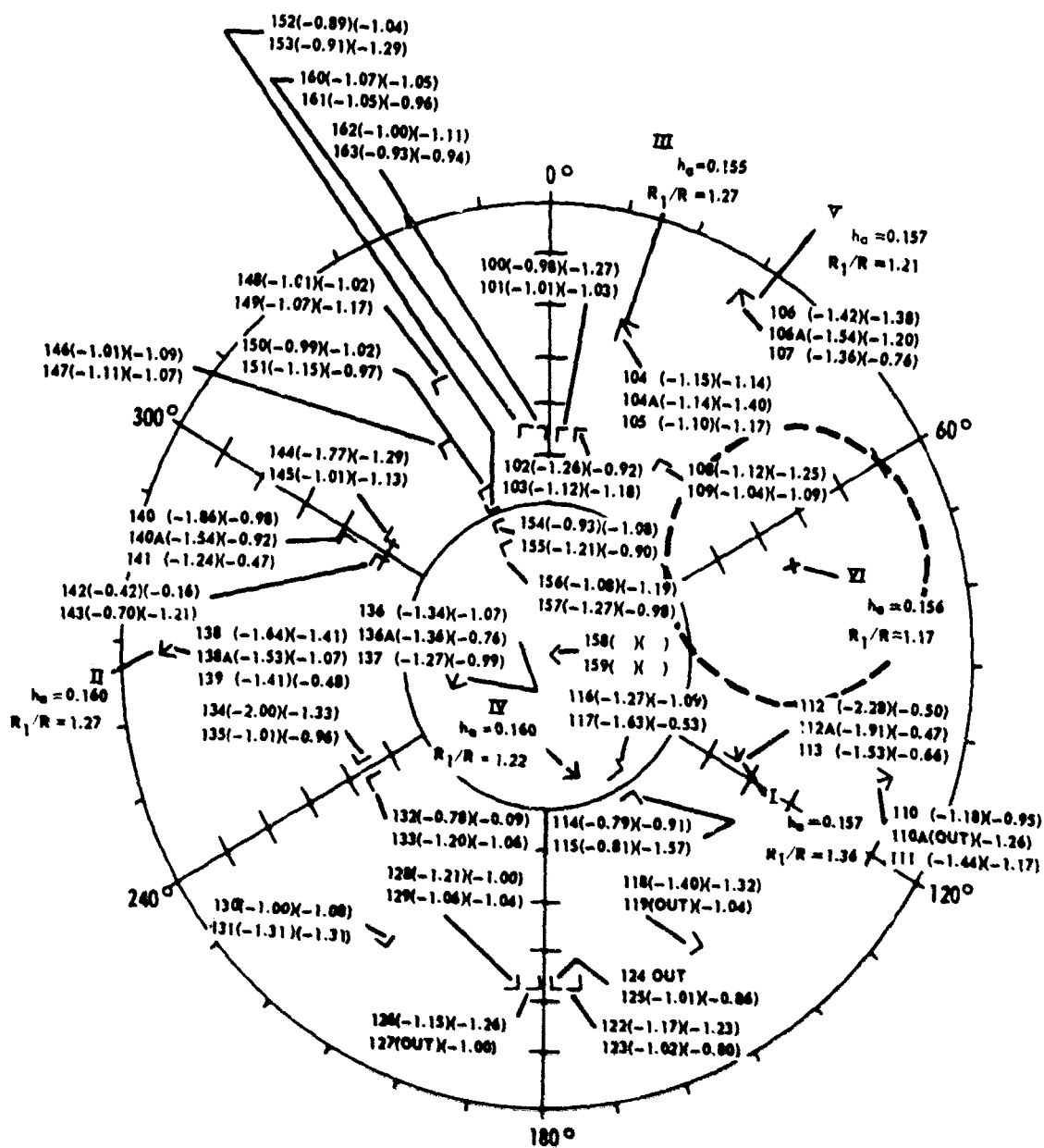
Figure 6h - Model SRS-2A

28

Figure 6i - Model SRS-3A

29
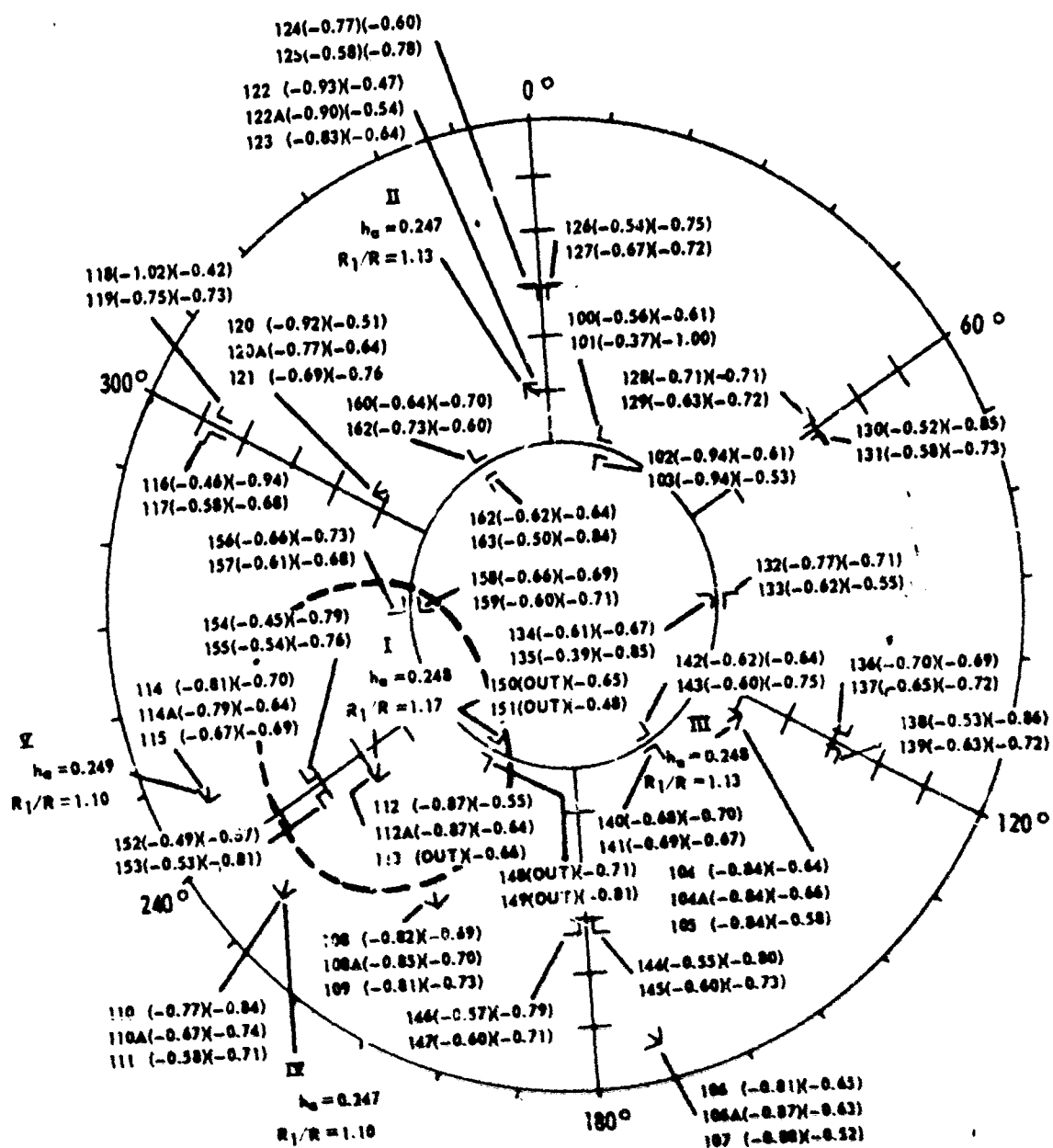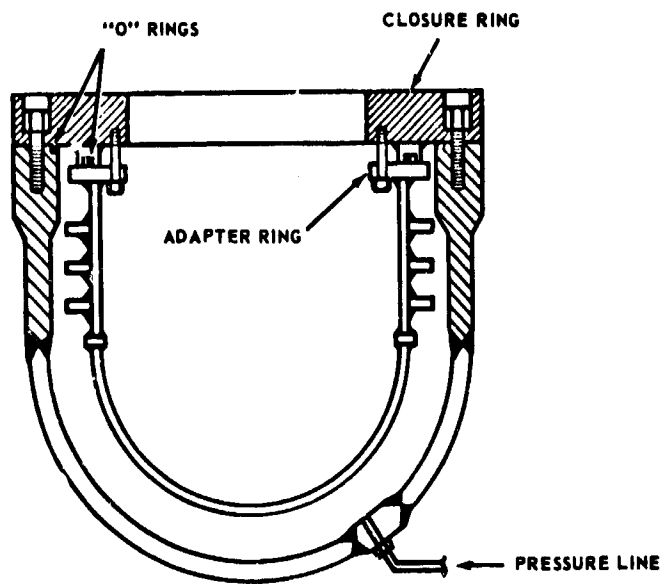
Figure 7a - 6-Foot Head Testing Tank
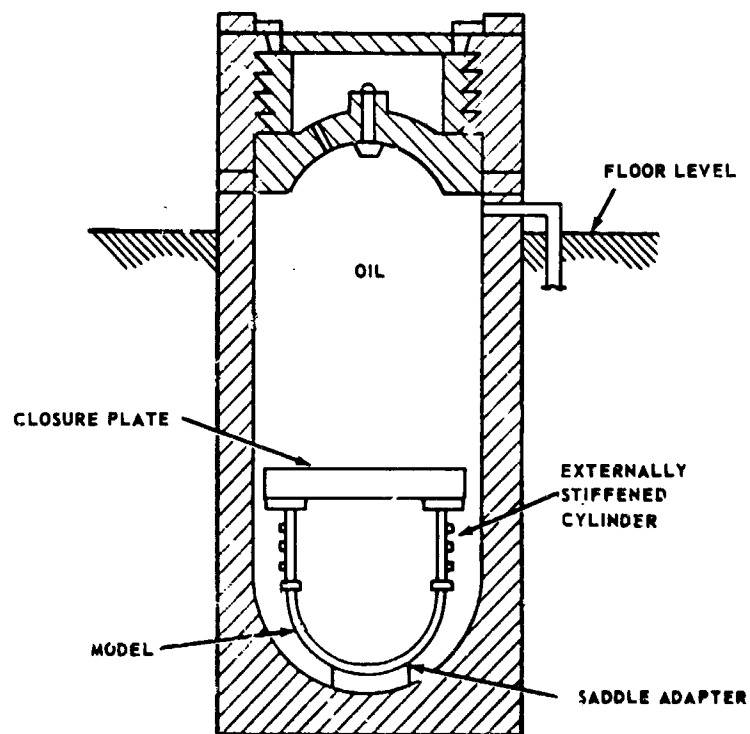
Figure 7b - 4-Foot Testing Tank

Figure 7 - Test Setup

30

31
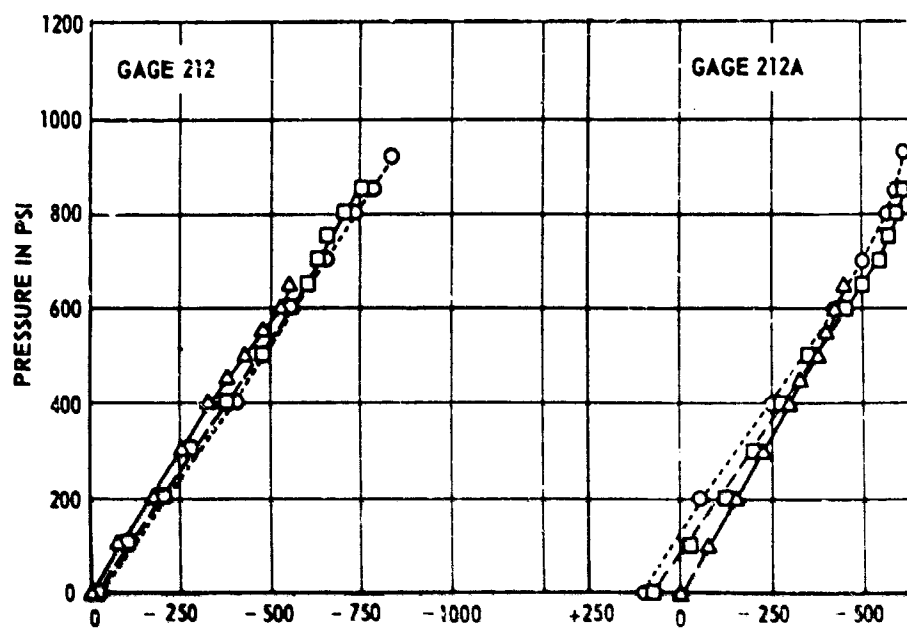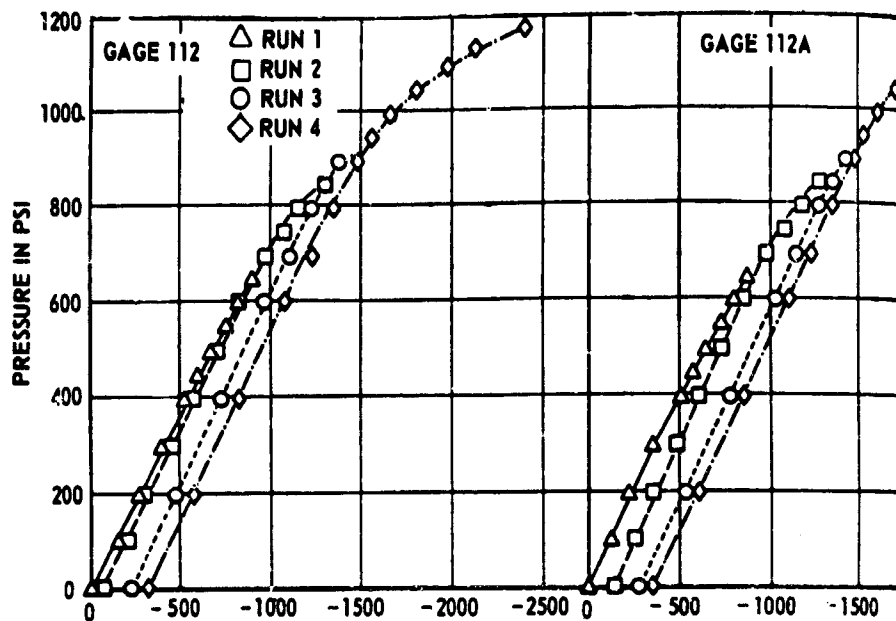
Figure 8 - Typical Pressure-Strain Plots

GAGE 113   GAGE 114   GAGE 115

-2000   0   -500   -1000   -1500   -2000   0   -250   -500   -750   -1000   +250   0   -250   -500   -750   -1000

STRAIN IN MICROINCH/INCH

GAGE 213   GAGE 214   GAGE 215

-50   0   -250   -500   -750   -1000   0   -250   -500   -750   -1000   0   -250   -500   -750   -1000   -1250

STRAIN IN MICROINCH INCH

Figure 8a - Model AF-1

GAGE 104

○ RUN 1
△ RUN 2
□ RUN 3

GAGE 116A

GAGE 204   GAGE 204A   GAGE 205   GAGE 216   GAGE 216A   GAGE

STRAIN IN μ IN.

32

GAGE 104A

−3000 −4000 −5000 −6000 −7000 −8000 −9000

0 −1000 −2000 −3000 −4000 −5000 −6000 −7000 −8000

STRAIN IN μ IN./IN.

GAGE 117

−3000 −4000 −5000 −6000 −7000 −8000 −9000

0 −1000 −2000 −3000 −4000 −5000 −6000 −7000 −8000

STRAIN IN μ IN./IN.

GAGE 205   GAGE 216   GAGE 216A   GAGE 217   GAGE 218   GAGE 219   GAGE 220   GAGE 221

1000   0   −1000   0   −1000   0   −1000   0   −1000   0   −1000   0   −1000   −2000   0   −1000   −2000   0   −1000

STRAIN IN μ IN. IN.

Figure 8b - Model

32

GAGE 105

GAGE 116

GAGE 118

GAGE 119

GAGE 120

GAGE 121

- 9000   0   - 1000   - 2000   - 3000   - 4000   - 5000   - 7000   - 3000

0   - 1000   - 2000   - 3000   - 4000

- 9000   0   - 1000   - 2000

0   - 1000   - 2000

0   - 1000

0   - 1000

GAGE 116

GAGE 119   GAGE 120   GAGE 121

Figure 6

MODEL AF-3

GAGE 100A

-8000   -9000   -10,000   0   -1000   -2000   -3000   -4000   -5000   -6000

STRAIN IN μ IN./IN.

GAGE 112   GAGE 112A

-8000   -9000   -10,000   -11,000   0   -1000   -2000   -3000   0   -1000

STRAIN IN μ IN./IN.

GAGE 212   GAGE 212A   GAGE 213

0   -1000   -2000   0   -1000   0   -1000

μ IN./IN.

Figure 8c - Model AF-3

GAGE 113

-7000   -8000   -9000   -10,000   -11,000

-2000   -3000   0   -1000   -2000

Figure 8d - :

54

GAGE 116A

0   0   − 2000   − 4000   − 6000

μ IN./IN.

GAGE 216A

− 2000

μ IN. IN.

lodel SRS-3

Figure 8e – Model SRS-4

35
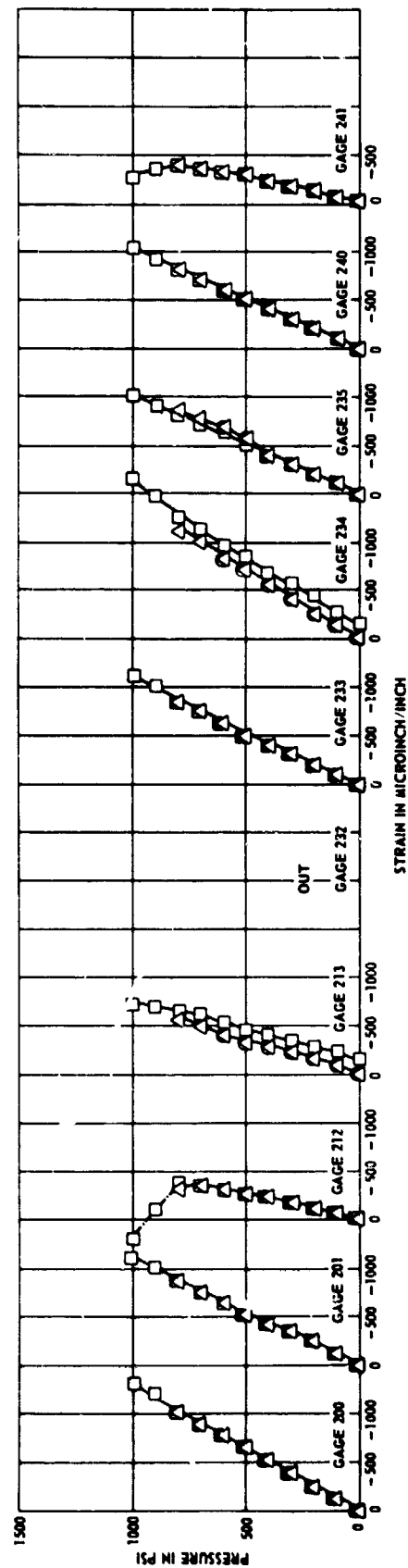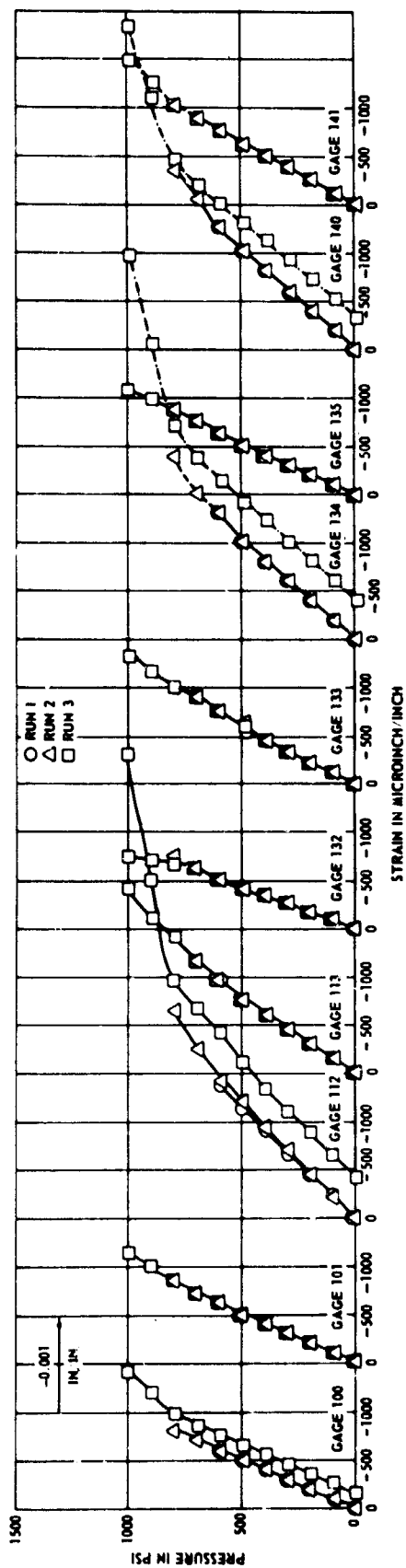
Figure 8f - Model SRS-2A
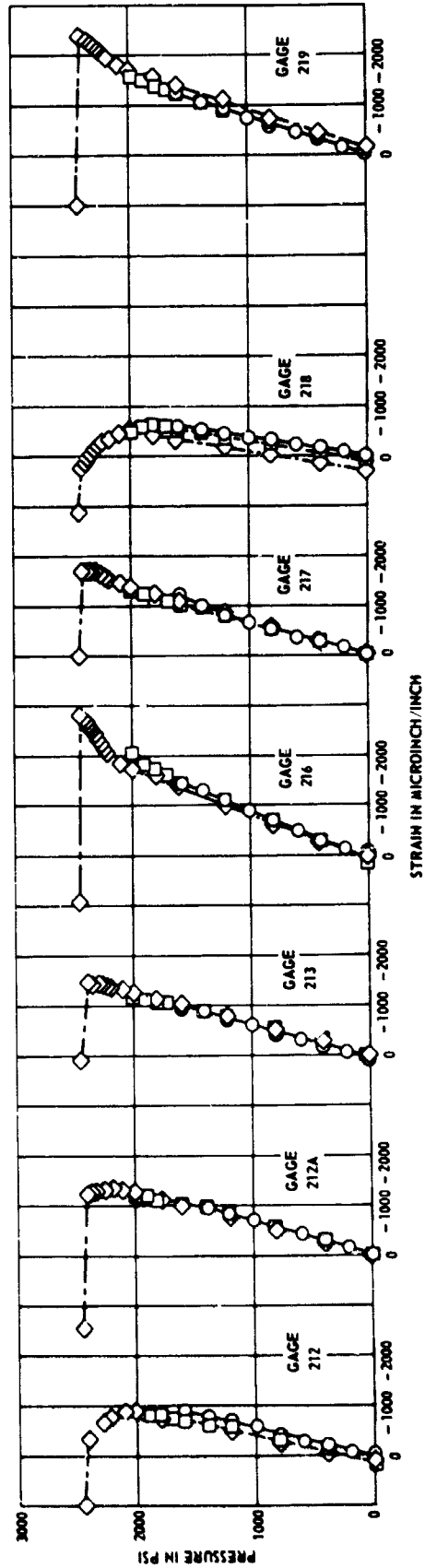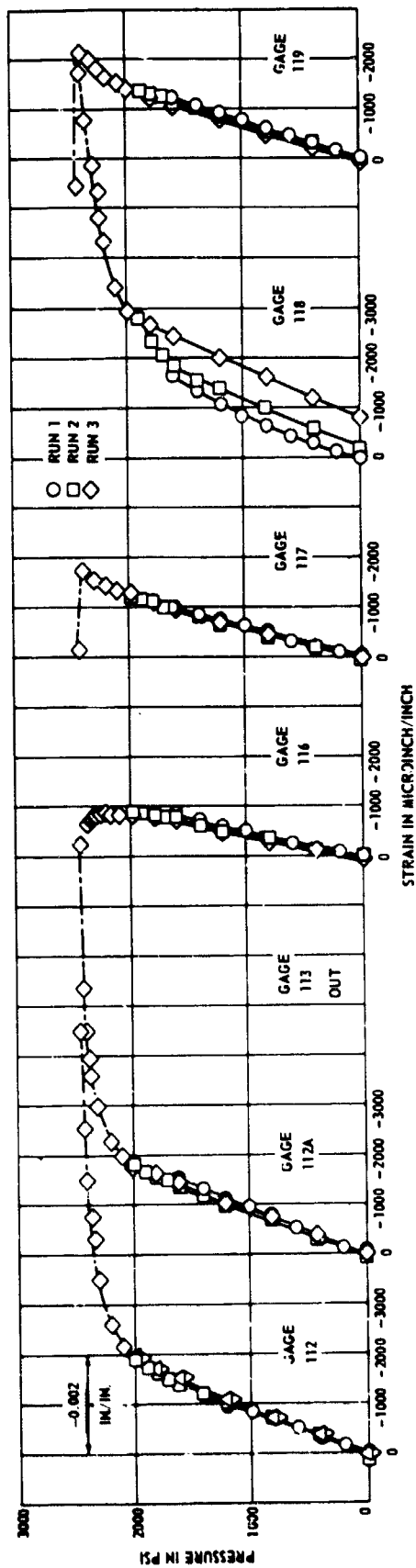
Figure 8g - Model SRS-3A

Figure 9 - Models After Collapse

PSD 327153

Figure 9b - Model AF-2

PSD 328109
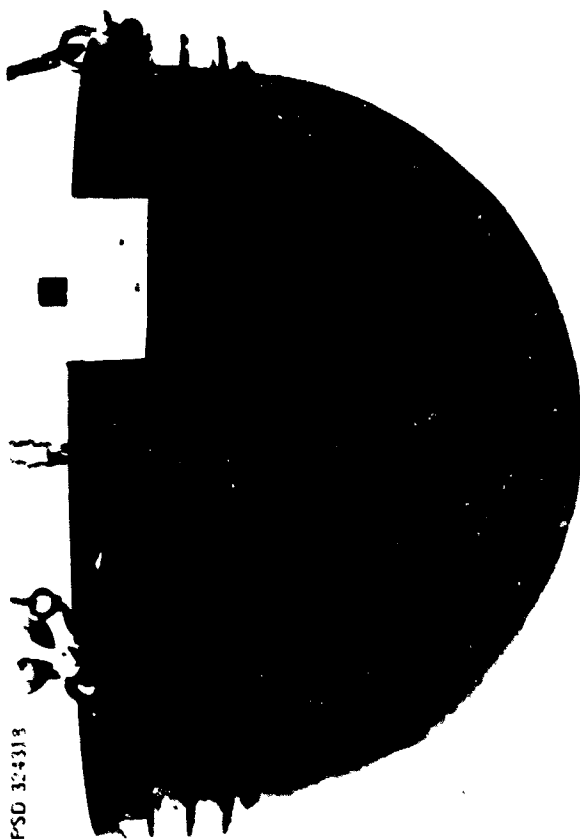
Figure 9c - Model AF-3

Figure 9a - Model AF-1

PSD 3243J9

38
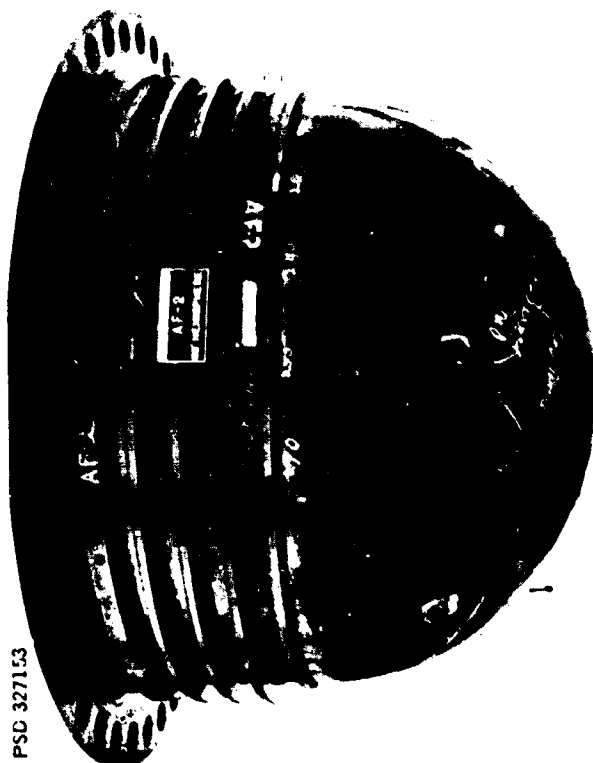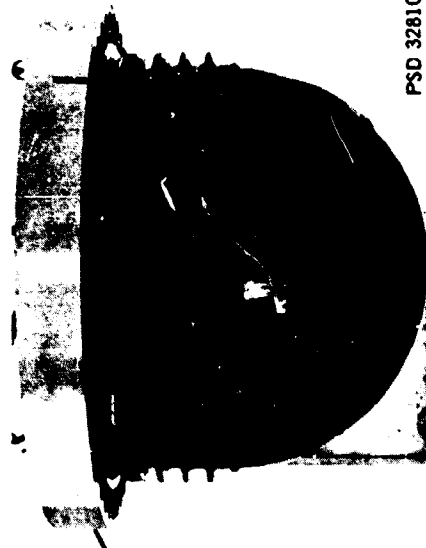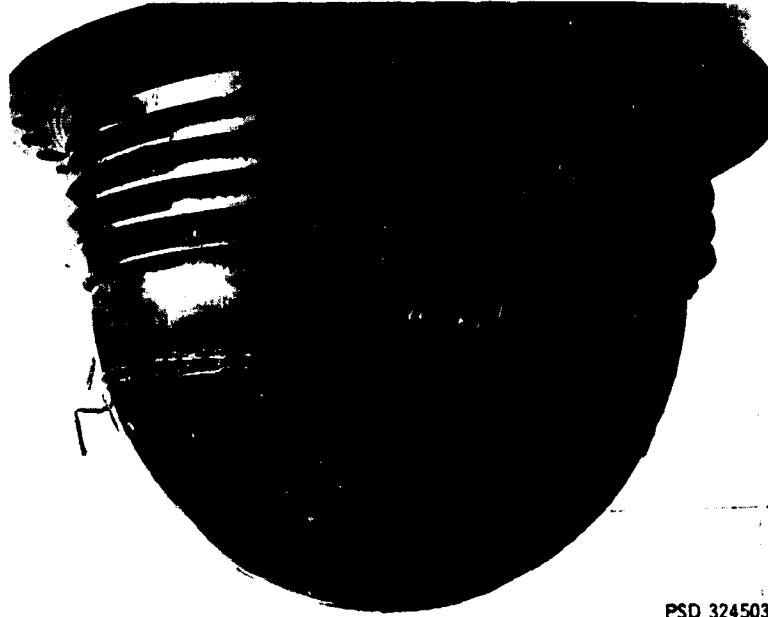
PSD 324503

Figure 9d - Model SRS-1
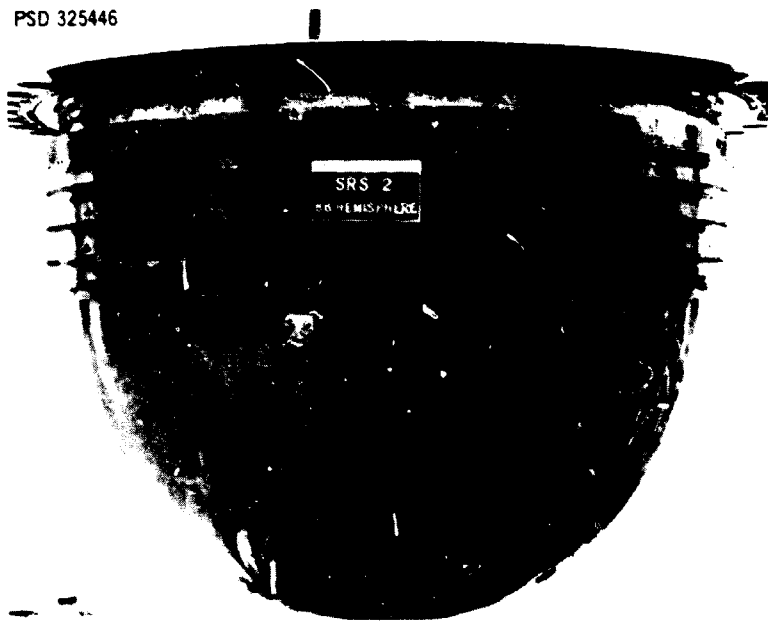
PSD 325446

SRS 2

Figure 9e - Model SRS-2
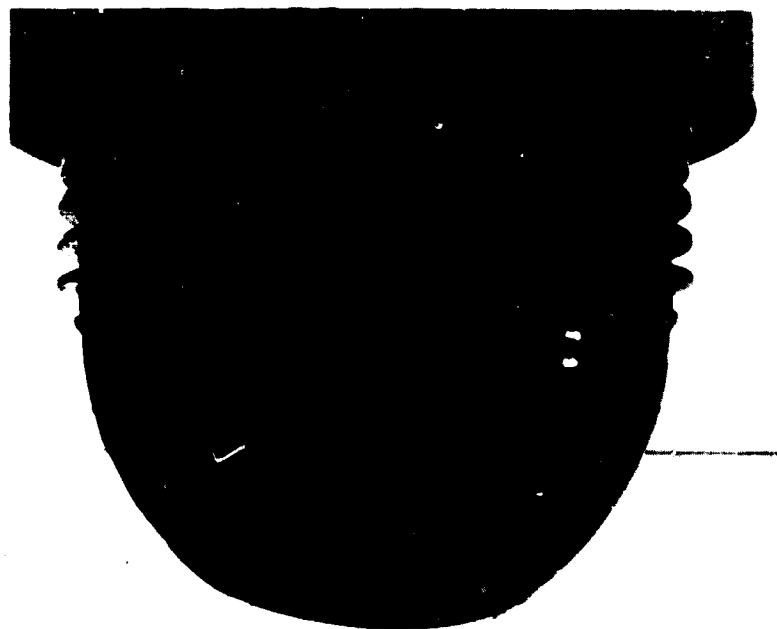
Figure 9f - Model SRS-3

Figure 9g - Model SRS-4

Figure 9h - Model SRS-2A

Figure 9i - Model SRS-3A

LOWER BOUND FOR STRESS RELIEVED HEMISPHERES

$P_c = P_3' = 0.84E \left(h/R_{10} \right)^2$

YIELD

SRS-4

LOWER BOUND FOR HEMISPHERES
WITH STRESS RELIEVED SEGMENTS

SRS-3A

AF-3

SRS-3

AF-2

LOWER BOUND FOR AS-FABRICATED HEMISPHERES

AF-1   SRS-2

SRS-2A

SRS-1

STRESS		30" DIAM. HEMISPHERES
● RELIEVED		
SEGMENTS		
STRESS		
■ RELIEVED		66" DIAM. HEMISPHERES
SEGMENTS		
NOT STRESS		
□ RELIEVED		

BASED ON AVERAGE THICKNESS h_a

AND LOCAL RADIUS IN AREA OF FAILURE

$(\theta_{CRIT} = 2.2)$

P_c = EXPERIMENTAL COLLAPSE PRESSURE

$P_y' = \dfrac{2 \sigma y \, h_a R_{1m}}{R_{10}^2}$

$P_3' = 0.84E \left(h_a/R_{10} \right)^2$

P_3'/P_y'

P_c, P_y'

Figure 10 - Nondimensional Plot of Experimental Results for
Fabricated HY-80 Steel Spherical Shells

42

TABLE 1
Compressive Yield Strengths

Model	Yield Strength in psi			
	Source of Yield Strength			
	Original Plate*	Coupon from Original Plate Stress Relieved with Model	Cold Formed Segment	Cold Formed and Stress Relieved Segment
AF-1	93,035			
AF-2	96,731			
AF-3	92,332			
SRS-1	95,951			
SRS-2	96,651	94,462		
SRS-3	95,453	94,789		
SRS-4	80,577			
SRS-2A	89,723		88,121	87,970
SRS-3A	90,830		90,117	90,417

*Used in calculations for P_y.

43

TABLE 2

Wall Thickness Readings

Model AF-2

Meridional Orientation in degrees

Circumferential Orientation in degrees	0°	15	30	45	60	75	90
0°	0.634	0.628	0.628	0.628	0.614	0.611	0.600
15	0.660	0.625	0.611	0.602	0.615	0.605	
30	0.625	0.627	0.667	0.667	0.616	0.605	
45		0.621	0.611	0.621	0.612		
60	0.625	0.618	0.624	0.626	0.617	0.606	
60*	0.630	0.615	0.635	0.628	0.615		
75		0.624	0.619	0.618	0.612		
90	0.645	0.619	0.618	0.614		0.608	
105		0.618	0.618	0.618			
120	0.631	0.625	0.635	0.628	0.612	0.625	0.609
120*	0.626	0.627	0.609	0.611	0.609		
135		0.619	0.609	0.610			
150	0.628	0.505	0.603	0.605	0.610	0.632	0.609
165		0.618	0.610	0.618			
180	0.625	0.626	0.632	0.622	0.609	0.631	0.618
180*	0.627	0.622	0.626	0.625	0.622		
195		0.612	0.610	0.618			
210	0.628	0.602	0.603	0.608	0.618	0.629	0.609
225		0.611	0.611	0.621			
240	0.619	0.628	0.628	0.632	0.625	0.625	0.614
240*	0.619	0.630	0.632	0.629	0.620		
255		0.612	0.620	0.617			
270	0.622	0.605	0.601	0.598	0.615	0.623	0.605
285		0.605	0.608	0.610			
300	0.611	0.610	0.620	0.616	0.605	0.620	0.605
300*	0.621	0.630	0.628	0.631	0.624		
315		0.610	0.609	0.612			
330	0.615	0.608	0.595	0.609	0.625	0.611	0.605
345		0.596	0.602	0.616			
360	0.620	0.610	0.628	0.622	0.612	0.612	0.605

$h_{AVG}=0.618$ $h_{MIN}=0.590$ $h_{MAX}=0.660$

Model AF-1

Meridional Orientation in degrees

Circumferential Orientation in degrees	0°	15	30	45	60	75	90
0°							0.395
15						0.392	
30						0.385	
45							
60					0.397	0.385	
60*					0.397		
75					0.405	0.390	
90					0.409	0.391	
105							
120				0.410			
120*				0.400			
135					0.396	0.388	
150							
165					0.401	0.392	
180							
180*							
195					0.395	0.385	
210							
225					0.392	0.385	
240							
240*							
255					0.396	0.386	
270							
285					0.390	0.390	
300							
300*							
315					0.395	0.380	
330							
345							
360							

$h_{AVG}=0.394$ $h_{MIN}=0.365$ $h_{MAX}=0.410$

44

Table 4 (Continued)

Model AF-

Circumferential Orientation in degrees vs Meridional Orientation in degrees

	0"	15	30	45	60-	60+	75	90
0+	0.735	0.742	0.756	0.730	0.710	0.746	0.725	0.720
15		0.730	0.728	0.728	0.745	0.725		
30	0.750	0.738	0.712	0.727	0.720			
45		0.740	0.725	0.732				
60-	0.745	0.748	0.753	0.747	0.720	0.733	0.730	
60+	0.738	0.732	0.729	0.740	0.731			
75		0.729	0.735	0.737				
90	0.752	0.731	0.727	0.728	0.730	0.740	0.730	
105		0.730	0.725	0.732				
120-	0.745	0.732	0.749	0.749	0.727	0.745	0.730	
120+	0.742	0.715	0.744	0.756	0.741			
135		0.733	0.740	0.740				
150	0.745	0.758	0.726	0.734	0.740	0.745	0.728	
165		0.740	0.740	0.750				
180-	0.745	0.750	0.760	0.763	0.740	0.745	0.730	
180+	0.735	0.740	0.745	0.741	0.740			
195		0.741	0.739	0.740				
210	0.745	0.742	0.730	0.730	0.724	0.750	0.730	
225		0.732	0.730	0.726				
240-	0.739	0.740	0.745	0.745	0.735	0.754	0.735	
240+	0.740	0.735	0.750	0.741	0.730			
255		0.740	0.729	0.736				
270	0.740	0.725	0.715	0.724	0.735	0.760	0.740	
285		0.741	0.729	0.731				
300-	0.745	0.752	0.756	0.748	0.730	0.749	0.733	
300+	0.740	0.750	0.756	0.756	0.749			
315		0.745	0.740	0.740				
330	0.745	0.735	0.710	0.729	0.735	0.750	0.733	
345		0.735	0.720	0.733				
360-	0.730	0.735	0.745	0.750	0.732			

h_{AVG}=0.7?9 | h_{MIN}=0.710 | h_{MAX}=0.780

Model SRS-1

Circumferential Orientation in degrees vs Meridional Orientation in degrees

	0+	15	30	45	60-	60+	75	90
0+	0.240	0.230	0.243	0.243	0.226	0.260	0.260	0.252
15		0.240	0.244	0.243				
30	0.243	0.242	0.244	0.243	0.230	0.253	0.258	
45		0.242	0.242	0.247				
60-	0.238	0.240	0.242	0.244	0.202	0.250	0.254	
60+	0.230	0.246	0.254	0.253	0.240			
75		0.239	0.252	0.254				
90	0.252	0.248	0.252	0.231	0.242	0.248	0.253	
105		0.255	0.257	0.255				
120-	0.246	0.244	0.246	0.246	0.230	0.247	0.254	
120+	0.255	0.256	0.256	0.250	0.228			
135		0.257	0.255	0.251				
150	0.251	0.255	0.255	0.253	0.228	0.256	0.262	
165		0.254	0.257	0.252				
180-	0.241	0.245	0.247	0.246	0.225	0.246	0.266	
180+	0.259	0.259	0.258	0.258	0.234			
195		0.258	0.255	0.252				
210	0.263	0.258	0.255	0.249	0.236	0.260	0.261	
225		0.256	0.256	0.252				
240-	0.256	0.254	0.248	0.252	0.231	0.260	0.260	
240+	0.250	0.242	0.254	0.254	0.234			
255		0.248	0.256	0.258				
270	0.253	0.254	0.250	0.258	0.246	0.265	0.260	
285		0.253	0.252	0.258				
300-	0.245	0.242	0.250	0.250	0.230	0.259	0.260	
300+	0.250	0.249	0.260	0.261	0.244			
315		0.251	0.256	0.256				
330	0.254	0.247	0.255	0.259	0.244	0.263	0.260	
345		0.241	0.357	0.258				
360-	0.246	0.228	0.244	0.2?6	0.237			

h_{AVG}=0.249 | h_{MIN}=0.282 | h_{MAX}=0.265

Table 2 (Continued)

Model SRS-3

Circumferential Orientation in degrees	Meridional Orientation in degrees							
	0+	15	30	45	60-	60+	75	90
0+	0.620	0.610	0.660	0.650	0.620	0.640	0.650	0.600
15		0.640	0.650	0.660				
30	0.680	0.640	0.650	0.610	0.630	0.640	0.650	
45		0.640	0.650	0.650				
60-	0.640	0.680	0.680	0.640	0.610	0.650	0.650	
60+	0.650	0.650	0.680	0.680	0.620			
75		0.660	0.570	0.650				
93	0.690	0.660	0.660	0.640	0.640	0.650	0.650	
105		0.660	0.670	0.670				
120-	0.620	0.550	0.640	0.670	0.650	0.610	0.650	
120+	0.640	0.650	0.670	0.680	0.640			
135		0.640	0.650	0.650				
150	0.650	0.640	0.640	0.640	0.620	0.660	0.650	
165		0.640	0.650	0.650				
180-	0.640	0.630	0.680	0.680	0.680	0.650	0.650	
180+	0.670	0.670	0.680	0.680	0.690			
195		0.650	0.670	0.650				
210	0.670	0.660	0.650	0.620	0.640	0.630	0.640	
225		0.650	0.680	0.650				
240-	0.650	0.660	0.700	0.640	0.600	0.600	0.650	
240+	0.640	0.660	0.660	0.650	0.570			
255		0.660	0.670	0.650				
270	0.700	0.680	0.660	0.650	0.640	0.640	0.650	
285		0.670	0.660	0.660				
300-	0.640	0.640	0.640	0.580	0.600	0.600	0.650	
300+	0.640	0.640	0.670	0.640	0.620			
315		0.650	0.650	0.650				
330	0.690	0.650	0.650	0.620	0.640	0.640	0.640	
345		0.660	0.660	0.650				
360-	0.620	0.630	0.610	0.640	0.640		0.640	

$h_{AVG}=0.649$ $h_{MIN}=0.580$ $h_{MAX}=0.700$

Model SRS-2

Circumferential Orientation in degrees	Meridional Orientation in degrees							
	0+	15	30	45	60-	60+	75	90
0+	0.361	0.386	0.390	0.381	0.376	0.364	0.386	0.369
15		0.382	0.386	0.382				
30	0.390	0.385	0.385	0.384	0.376	0.374	0.385	
45		0.385	0.390	0.392				
60-	0.378	0.384	0.391	0.381	0.379	0.375	0.380	
60+	0.380	0.375	0.383	0.390	0.365			
75		0.382	0.383	0.389				
90	0.384	0.376	0.380	0.386	0.370	0.360	0.386	
105		0.376	0.383	0.390				
120-	0.371	0.370	0.381	0.383	0.364	0.377	0.383	
120+	0.378	0.387	0.388	0.376	0.375			
135		0.386	0.390	0.390				
150	0.394	0.380	0.390	0.390	0.381	0.381	0.381	
165		0.384	0.388	0.369				
180-	0.380	0.375	0.387	0.385	0.376	0.381	0.387	
180+	0.383	0.390	0.385	0.380	0.372			
195		0.389	0.386	0.386				
210	0.394	0.390	0.387	0.385	0.373	0.366	0.390	
225		0.390	0.390	0.386				
240-	0.384	0.381	0.385	0.386	0.365	0.376	0.380	
240+	0.391	0.391	0.394	0.382	0.367			
255		0.387	0.390	0.385				
270	0.384	0.379	0.385	0.388	0.367	0.377	0.379	
285		0.392	0.394	0.386				
300-	0.385	0.372	0.390	0.380	0.364	0.360	0.384	
300+	0.390	0.390	0.392	0.369	0.365			
315		0.386	0.389	0.384				
330	0.391	0.385	0.384	0.381	0.361	0.370	0.382	
345		0.385	0.386	0.384				
360-	0.379	0.383	0.380	0.362	0.362			

$h_{AVG}=0.381$ $h_{MIN}=0.360$ $h_{MAX}=0.396$

46

Table 2 (Continued)

Model SRS-4

Meridional Orientation in degrees

Circumferential Orientation in degrees	0°	15	30	45	60⁻	60⁺	75	90
0°	0.721	0.723	0.746	0.737	0.714	0.742	0.731	0.724
15		0.730	0.732	0.735	0.712	0.742	0.729	
30	0.739	0.730	0.712	0.729	0.712			
45		0.725	0.729	0.723	0.702	0.730	0.732	
60⁻	0.721	0.723	0.698	0.729	0.719			
60⁺	0.735	0.735	0.735	0.731	0.719			
75		0.735	0.736	0.733	0.715	0.734	0.732	
90	0.741	0.734	0.730	0.731	0.715			
105		0.732	0.740	0.741	0.722	0.731	0.719	
120⁻	0.732	0.744	0.750	0.741	0.690			
120⁺	0.715	0.700	0.695	0.685	0.690			
135		0.722	0.720	0.710	0.720	0.729	0.722	
150	0.730	0.722	0.720	0.709	0.720			
165		0.722	0.722	0.722	0.698	0.740	0.729	
180⁻	0.718	0.712	0.721	0.709	0.698			
180⁺	0.714	0.727	0.740	0.741	0.700			
195		0.722	0.731	0.732	0.712	0.720	0.726	
210	0.739	0.730	0.721	0.728	0.712			
225		0.729	0.730	0.731	0.720	0.730	0.730	
240⁻	0.721	0.720	0.740	0.738	0.720			
240⁺	0.720	0.719	0.728	0.730	0.714			
255		0.730	0.729	0.712	0.713	0.727	0.730	
270	0.721	0.722	0.720	0.726	0.713			
285		0.725	0.725	0.729	0.709	0.735	0.730	
300⁻	0.718	0.732	0.730	0.731	0.709			
300⁺	0.731	0.740	0.730	0.739	0.734			
315		0.732	0.736	0.735	0.715	0.743	0.735	
330	0.741	0.730	0.723	0.732	0.715			
345		0.731	0.732	0.735				
360⁻	0.729	0.734	0.720	0.713				

h_AVG=0.726   h_MIN=0.685   h_MAX=0.750

Model SRS-4

Model SRS-2A

Meridional Orientation in degrees

Circumferential Orientation in degrees	0⁺	15	30	45	60⁻	60⁺	75	90
0⁺	0.155	0.156	0.157	0.157	0.156	0.162	0.154	0.154
15		0.155	0.153	0.153	0.153	0.161	0.154	
30	0.158	0.159	0.152	0.153	0.156			
45		0.155	0.154	0.156	0.156	0.158	0.155	
60⁻	0.155	0.158	0.159	0.158	0.157			
60⁺	0.154	0.156	0.158	0.156	0.156			
75		0.156	0.157	0.154	0.157	0.160	0.155	
90	0.162	0.156	0.150	0.152	0.157			
105		0.157	0.154	0.155	0.157	0.160	0.154	
120⁻	0.159	0.159	0.161	0.158	0.159			
120⁺	0.156	0.159	0.160	0.159	0.159			
135		0.155	0.154	0.156	0.161	0.160	0.154	
150	0.158	0.154	0.154	0.156	0.161			
165		0.157	0.156	0.159	0.160	0.160	0.155	
180⁻	0.153	0.160	0.161	0.160	0.160			
180⁺	0.155	0.154	0.158	0.158	0.159			
195		0.156	0.154	0.157	0.159	0.161	0.154	
210	0.158	0.152	0.150	0.154	0.159			
225		0.155	0.154	0.157	0.159	0.162	0.154	
240⁻	0.153	0.156	0.157	0.158	0.162			
240⁺	0.159	0.160	0.163	0.162	0.162			
255		0.159	0.158	0.158	0.163	0.162	0.155	
270	0.162	0.158	0.155	0.157	0.163			
285		0.160	0.158	0.161	0.162	0.161	0.155	
300⁻	0.159	0.161	0.163	0.163	0.160			
300⁺	0.160	0.162	0.164	0.160	0.160			
315		0.161	0.159	0.159	0.161	0.155		
330	0.162	0.160	0.156	0.157	0.161			
345		0.161	0.158	0.159				
360⁻	0.160	0.162	0.162	0.161	0.161			

h_AVG=0.158   h_MIN=0.150   h_MAX=0.164

Model SRS-2A

47

Table 2 (Continued)

Meridional Orientation in degrees

	0+	15	30	45	60-	60+	75	90
0+	0.252	0.251	0.252	0.251	0.251	0.251	0.244	0.242
15		0.247	0.242	0.244				
30	0.244	0.242	0.240	0.244	0.248	0.251	0.244	
45		0.243	0.242	0.244				
60-	0.250	0.250	0.240	0.249	0.250	0.252	0.243	
60+	0.252	0.251	0.252	0.251	0.254			
75		0.247	0.246	0.247				
90	0.254	0.246	0.240	0.240	0.250	0.250	0.244	
105		0.247	0.244	0.244				
120-	0.252	0.250	0.250	0.251	0.249	0.250	0.243	
120+	0.250	0.250	0.250	0.247	0.248			
135		0.245	0.242	0.243				
150	0.254	0.242	0.240	0.240	0.246	0.251	0.243	
165		0.243	0.242	0.241				
180-	0.250	0.250	0.248	0.249	0.249	0.254	0.243	
180+	0.249	0.248	0.251	0.250	0.251			
195		0.244	0.246	0.244				
210	0.252	0.244	0.240	0.243	0.252	0.256	0.244	
225		0.247	0.242	0.244				
240-	0.247	0.247	0.248	0.248	0.248	0.251	0.244	
240+	0.252	0.250	0.250	0.249	0.250			
255		0.247	0.243	0.244				
270	0.254	0.244	0.240	0.241	0.247	0.249	0.244	
285		0.247	0.242	0.241				
300-	0.251	0.250	0.249	0.250	0.251	0.252	0.245	
300+	0.252	0.253	0.250	0.248	0.249			
315		0.249	0.251	0.247				
330	0.251	0.244	0.246	0.240	0.247	0.249	0.245	
345		0.246	0.240	0.241				
360-	0.251	0.249	0.250	0.250	0.248			

Circumferential Orientation in degrees

$h_{AVG} = 0.247$ $h_{MIN} = 0.240$ $h_{MAX} = 0.256$

Model SRS-3A

48

TABLE 3

Local Geometry and Comparison of Calculated and Measured Membrane Stresses and Collapse Pressures

Model	Area	h_a inch	$\frac{R_1}{R}$	Calculated Max. Memb. Stress Sens. 1 psi/psi	Measured Max. Memb. Stress Sens. 2 psi/psi	Ratio of Calc. to Meas. Stress	Exp. Collapse Pressure, psi
	I	0.395	1.32	55.72	50.67	1.100	
	II*	0.391	1.23	52.50	53.14	0.988	
AF-1	III	0.393	1.23	52.23	50.27	1.039	1260
	IV	0.390	1.19	50.94	51.15	0.996	
	V	0.398	1.18	49.52	47.01	1.053	

AF-?	I	0.623	1.32	35.65	33.55	1.053	2240
	II	0.630	1.26	33.70	33.50	1.006	
	III	0.615	1.26	34.50	31.68	1.089	
	IV	0.609	1.25	34.56	28.10	1.229	
	V	0.629	1.23	32.96	31.90	1.033	
	VI*	0.627	1.23	33.07	31.60	1.047	
AF-3	I*	0.724	1.32	30.78	33.11	0.929	2700
	II	0.728	1.26	29.26	29.70	0.985	
	III	0.730	1.22	28.28	29.44	0.961	
	IV	0.728	1.20	27.90	29.54	0.944	
	V	0.722	1.19	27.90	30.69	0.909	
SRS-1	I*	0.252	1.76	115.50	111.4	1.037	490
	II	0.250	1.25	82.90	84.5	0.981	
	III	0.255	1.24	80.64	77.4	1.042	
	IV	0.252	1.23	80.95	80.5	1.006	
	V	0.243	1.19	80.21	92.0	0.872	
SRS-2	I	0.389	1.20	51.34	gage out	---	1575
	II	0.385	1.20	51.87	50.42	1.028	
	III	0.389	1.19	50.93	50.68	1.005	
	IV	0.390	0.17	49.96	gage out	---	
	V	0.381	1.15	50.26	50.17	1.002	
	VI*	0.387	1.11	47.80	no gage	---	
SRS-3	I	0.620	1.36	36.85	32.69	1.127	2360
	II	0.655	1.34	34.42	35.96	0.957	
	III*	0.620	1.23	33.40	36.80	0.908	
	IV	0.660	1.19	30.42	34.00	0.895	
	V	0.660	1.17	29.93	36.22	0.826	
SRS-4	I	0.733	1.39	31.95	26.06	1.226	2850
	II	0.737	1.32	30.22	26.34	1.147	
	III	0.726	1.20	27.94	26.18	1.067	
	IV	0.721	1.17	27.45	26.25	1.046	
	V	0.724	1.16	27.11	25.85	1.049	
	VI*	0.724	1.12	26.20	24.97	1.049	
					56.79	1.152	

	IV	0.660	1.19	30.42	34.00	0.895	
	V	0.660	1.17	29.93	36.22	0.826	
SRS-4	I	0.733	1.39	31.95	26.06	1.226	
	II	0.727	1.32	30.22	26.34	1.147	
	III	0.726	1.20	27.94	26.18	1.067	2850
	IV	0.721	1.17	27.45	26.25	1.046	
	V	0.724	1.16	27.11	25.85	1.049	
	VI*	0.724	1.12	26.20	24.97	1.049	
SRS-2A	I	0.157	1.36	65.43	56.79	1.152	
	II	0.160	1.27	59.39	59.59	0.997	
	III	0.155	1.27	62.27	51.95	1.199	1060
	IV	0.160	1.22	57.96	gage out	---	
	V	0.157	1.21	58.21	57.79	1.007	
	VI*	0.156	1.17	56.96	no gage	---	
SRS-3A	I*	0.248	1.17	36.09	gage out	---	
	II	0.247	1.13	35.00	31.32	1.117	
	III	0.248	1.13	34.86	31.74	1.098	2440
	IV	0.247	1.10	34.08	32.75	1.041	
	V	0.249	1.10	33.81	31.45	1.075	

1. The calculated stress sensitivities are determined from the equation

$$\text{Stress sensitivity} = \frac{R_{10}^2}{2 h_a R_{1m}}$$

2. The measured stress sensitivities are based on the average of the strain-sensitivity readings taken on the inside and outside surfaces of the shell. The strain sensitivity is defined as the slope of the portion of the pressure-strain diagram which is linear. Measured stress sensitivities are determined from the expression

$$\text{Stress sensitivity} = \frac{\varepsilon}{0.2}\left[\frac{\varepsilon_1 + \varepsilon_3}{1-\mu} + \frac{1}{1+\mu}\sqrt{\left(\varepsilon_1 - \varepsilon_3\right)^2 + \left[2\varepsilon_2 - \left(\varepsilon_1 + \varepsilon_3\right)\right]^2}\right]$$

where ε_1, ε_2, and ε_3 are the average strain sensitivities at the 0-, 45-, and 90-deg orientation in a three-element rosette.

*Failure area.

TABLE 4

Comparison of Predicted and Experimental Collapse Pressures

Model	Failure Area	P_{pred}*	P_{exp}	$\dfrac{P_{exp}}{P_{pred}}$
AF-1	II	1035	1260	1.22
AF-2	VI	2076	2240	1.08
AF-3	I	2460	2700	1.10
SRS-1	I	465	490	1.04
SRS-2	VI	1280	1575	1.23
SRS-3	III	2007	2360	1.18
SRS-4	VI	2207	2850	1.29
SRS-2A	VI	880	1060	1.20
SRS-3A	I	2001	2440	1.22

*P_{pred} is determined by calculating P_3^- and P_y^- at Area I, the "critical" area with respect to h_a/R_1, and then using the proper lower bound curve in Figure 10 to get P_c or P_{pred}. The data points in Figure 10 were based on the local geometry in the "failure area."

REFERENCES

1. Kiernan, T.J. and Nishida, K., "The Buckling Strength of Fabricated HY-80 Steel Spherical Shells," David Taylor Model Basin Report 1721 (Jul 1966).

2. Costello, M.G. and Nishida, K., "The Inelastic Buckling Strength of Fabricated HY-80 Steel Hemispherical Shells," NSRDC Report 2304 (Apr 1967).

3. Krenzke, A. and Kiernan, T.J., "The Effect of Initial Imperfections on the Collapse Strength of Deep Spherical Shells," David Taylor Model Basin Report 1757 (Feb 1965).

4. Costello, M.G., "The Effect of Mismatch on the Collapse Strength of Machined Hemispherical Shells," NSRDC Report 3383 (Jul 1970).

DOCUMENT CONTROL DATA - R & D

Security classification of title, body of abstract and indexing annotation must be entered when the overall report is classified

1. ORIGINATING ACTIVITY (Corporate author)	2a. REPORT SECURITY CLASSIFICATION
Naval Ship Research and Development Center Washington, D. C. 20034	Unclassified
	2b. GROUP

3. REPORT TITLE

THE EFFECT OF RESIDUAL STRESSES ON THE BUCKLING STRENGTH OF FABRICATED HY-80 STEEL HEMISPHERICAL SHELLS

4. DESCRIPTIVE NOTES (Type of report and inclusive dates)

Final Report

5. AUTHOR(S) (First name, middle initial, last name)

M. G. Costello

6. REPORT DATE	7a. TOTAL NO. OF PAGES	7b. NO. OF REFS
October 1970	54	4

8a. CONTRACT OR GRANT NO	9a. ORIGINATOR'S REPORT NUMBER(S)
b. PROJECT NO SF 35.422.210, Task 15054	
c.	9b. OTHER REPORT NO(S) (Any other numbers that may be assigned this report)
d.	

10. DISTRIBUTION STATEMENT

This document is subject to special export controls and each transmittal to foreign governments or foreign nationals may be made only with prior approval of Naval Ship Research and Development Center, Code 700.

11. SUPPLEMENTARY NOTES	12. SPONSORING MILITARY ACTIVITY
	Naval Ship Systems Command

13. ABSTRACT

Hydrostatic tests were conducted on nine fabricated HY-80 steel hemispheres to observe the effects of residual stresses from cold forming and welding on elastic response and collapse strength. Non-dimensionalized collapse data indicated that residual stresses due to welding play a significant part in the collapse strength of fabricated HY-80 steel hemispheres.

DD FORM **1473** (PAGE 1)

S/N 0101-807-6801

62

14 KEY WORDS	LINK A		LINK B		LINK C	
	ROLE	WT	ROLE	WT	ROLE	WT
Spherical Shells						
Initial Imperfections						
Residual Stresses						
Buckling						
Elastic Behavior						
Inelastic Behavior						

DD FORM 1 NOV 65 1473 (BACK)
(PAGE 2)